Exoelectrogenic Biofilm Growth in Shearing Flows

by

Akhenaton-Andrew Dhafir Jones, III

S.B., Department of Mathematics, Massachusetts Institute of Technology (2010)
S.B., Department of Mechanical Engineering, Massachusetts Institute of Technology (2010)
S.M., Department of Mechanical Engineering, Massachusetts Institute of Technology (2014)

Submitted to the Department of Mechanical Engineering
in partial fulfillment of the requirements for the degree of

Doctor of Philosophy

at the

MASSACHUSETTS INSTITUTE OF TECHNOLOGY

February 2018

Author .....
Department of Mechanical Engineering
November 01, 2017

Certified by .....
Cullen R. Buie
Associate Professor of Mechanical Engineering and the Esther and Harold E. Edgerton Career Development Chair
Thesis Supervisor

Accepted by .....
Rohan Abeyaratne
Quentin Berg Professor of Mechanics
Chairman, Department Committee on Graduate Theses

Exoelectrogenic Biofilm Growth in Shearing Flows

by

Akhenaton-Andrew Dhafir Jones, III

Submitted to the Department of Mechanical Engineering
on November 01, 2017, in partial fulfillment of the
requirements for the degree of
Doctor of Philosophy

Abstract

Microbial biofouling occurs when a biofilm adheres to materials involved in liquid transport causing economic loss through corrosion and drag losses on ship hulls, and in oil and food distribution. Microorganisms interacting with surfaces under these open channel flows contend with high shear rates and active transport to the surface. The metallic surfaces they interact with carry charge at various potentials that are little addressed in literature. We demonstrate for the first time that mass transport limiting current, chronoamperometry, and cyclic voltammetry in a rotating disk electrode are ideal for studying adhesion of microbes to metallic surfaces under shear. We study the adhesion of *Escherichia coli*, *Bacillus subtilis*, and 1 μm silica microspheres over a range of shear stresses. Our results agree with literature on red blood cells in rotating disk electrodes and deposition rates of *B. subtilis* and *E. coli* from optical systems, and show that we can quantify changes in active electrode area by bacteria adhesion and protein secretion. Our methodology measures changes in area instead of mass simultaneously providing measurements of the protein binding step that initiates biofilm formation. Unlike fluorescence microscopy, these methods are in vivo and apply to a larger range of problems than on-chip flow devices.

We also use the rotating disk system to present the first study of how electroactive biofilms adapt to shear stress over time. These biofilms are unique in that they do not rely on electron acceptor diffusion as they are "wired" to the electron acceptor, leading to thicker biofilms. Furthermore, it is possible to use the current produced by the biofilms as a proxy for metabolic respiration. We measure current, open circuit potential, electron diffusion current, electrochemical impedance, and formal potential throughout the course of seven days of *Geobacter sulfurreducens* forming a biofilm on a graphite disk exposed to three different shear stresses (1, 0.1, 0.01 Pa) and fixed mass flux. We image the resulting biofilm to measure biofilm thickness, porosity, and surface roughness. We find that high shear rates lead to faster start-up times and higher current, and by proxy higher metabolic rates, at the cost of long term sustainability of this current. We also find that there was no statistical difference in thickness or surface roughness between biofilms of different stresses. Similar to previous work, we propose that the lack of stability is due to the absence of waste

removal.

Our results are the first to show that the rotating disk system can be used investigate biofilm's development, metabolism, and structure from initiation to decay in vivo under fluid shear stress and electrical stress conditions that occur in our engineered environments. Future work using this system can include increased sampling frequency to understand start-up behavior and analysis of how mixed cultures modify adhesion, start-up respiration rates, and waste removal.

Thesis Supervisor: Cullen R. Buie
Title: Associate Professor of Mechanical Engineering and the Esther and Harold E. Edgerton Career Development Chair

Acknowledgments

I would like to thank my advisor, Professor Cullen R. Buie for spending more time with me than is likely advisable as both my research supervisor in this work and as the Associate housemaster when I served as a graduate resident tutor in Maseeh Hall. As the 5th graduate student to join his lab, he has set an invaluable example and given great insight into the tenure process at what is likely one of the hardest places to obtain tenure while raising a family, being an engaging and caring teacher and a research leader.

I would like to thank my committee members, Profs Annette "Peko" Hosoi and Ruben Juanes for pulling me back from the brink of numerical modeling and reminding me of the power of dimensional analysis and its proper usage.

I would like to thank the members of the Laboratory for Energy & Microsystems Innovation, Will Braff for teaching me about *Geobacter sulfurreducens* culturing, I now understand one of the reasons you switched projects; Zhifei Ge for teaching me about aerobic culturing; Alisha Schor for teaching me me about liquid handling and putting up with my OCD desk behavior; Qianru Wang for putting up with my slow culturing schedules and walking through debugging phases. In addition to Aron Blasei, Tim Palmer, Youngsoo Joung, Jeff Moran, Naga Dingari, Kameron Conforti, Laura Gilson, Paulo Garcia, Rameech McCormack, Chelsea Cataina, and Chris Vaina. My UROPs, Ryan Karnish, Kristina Greenwood, Ty Ingram, and Meera Gregorson: hopefully I taught you something. The administrators of the lab: Mieke Moran and Maral Banosian, we couldn't have done anything without you

I would like to thank Dr. Valerie Watson and Wendy Salmon at the Keck Center for Microscopy in the Whitehead Institute for Biomedical Research for tips and tricks for drying and imaging biofilms. All indepth pictures were obtained using some part of their insight.

I would like to acknowledge the Academy of Courageous Minority Engineers, ACME. While Wil E Coyote taught most people to never trust ACME products, this group kept me going, kept me honest, kept me humble, kept me pushing and focused

and made sure I did not get lost. In the same breath, I would like to acknowledge the Black Graduate Student Association, and the rest of the black community at MIT. It is tough to keep pushing forward in academic pursuits when our very lives continue to be devalued and dehumanized, you have allowed me to just be me, every facet of me without worry and fear of threat and at the same time providing comfort and understanding of those fears. I'd list names but I might forget some.

I would like to acknowledge some my mentors, Profs' Sanjay Sarma, John Brisson, Gabriella Carolini, Wes Harris, Philip Clay and Drs Benita Comeau and Barbara Hughey for their continuous encouragement for me entering into the academy; to balance my health, work, and family; to make a difference teaching and researching to make the world a more just society.

I would like to acknowledge the Alfred P Sloan Foundation - University Center for Exemplary Mentorship for support in my last two years. Specifically Eboney Hearn, Gloria Anglon, Leslie Kolodziejski for teaching me about the academic job market.

I would like to thank my parents Andrew D. and Julie L. Jones for my birth; their love in face of precociousness that lasted a little too long; for raising me with an open mind. I would also like to thank my sister Khoranhalai Juliealma Lyki'El Melba Jones for constantly reminding me how much fun hands on work is. I would like to thank my sister Khoranalai Anjulique Josephine Chestina Jones for editing at least 3 papers, better than some professional editorial services I hired. My grandparents Alma and James Lee, who shuttled and sheltered me during an internship at Oak Ridge which lead to interesting insights sprinkled throughout in addition to my first publication.

I would like to thank my wife, Cristen Blair Jones, the face that smiles down on me from my cabinet above my monitor. For the following, abbreviated, reasons: putting up with, sometimes sitting with me during late nights in lab; for helping me smile in 0 °C weather; for trips to Ithaca; for getting me into November Project, Crossfit, Edward Tufte, and who knows what else. For her love, support, and multiple photoshop edits and illustrator wizardry.

Contents

List of Figures

List of Tables

List of Symbols

The next list describes several symbols that will be later used within the body of the document

μ	Dynamic viscosity of solvent	$\mathrm{M\,L^{-1}T^{-1}}$
ν	Kinematic viscosity of solvent	$\mathrm{L^2T^{-1}}$
Ω	Frequency of EIS scan	T^{-1}
ω	Rotation of disk	$\mathrm{T^{-1}}$
ϕ	Volume fraction of total solid volume to fluid volume	[]
τ_p	Shear stress on porous media	$\mathrm{M\,L^{-1}\,T^{-2}}$
$\tilde{\tau}_p$	Dimensionless shear stress of particle packed pipe, ratio of shear stress to fluid inertia	[]
A	Projected area of disk	$\mathrm{L^2}$
A_r	Area of reactor	$\mathrm{L^2}$
c_∞	Bulk concentration of substrate	$\mathrm{M\,L^{-3}}$
D_0	Diffusivity of substrate	$\mathrm{L^2T^{-1}}$
D_p	Pore scaled diameter of a particle packed pipe	[L]
F	Faraday's constant	$96\,485.332\,89\,\mathrm{C\,mol^{-1}}$
i	Current	§A

i_{lim}	Limiting current	$\S A$
K	Kozney constant	[]
k_p	Permeability	L^2
L	Length of pipe	[L]
N	Flux of substrate to the disk	$\mathrm{M\,L^{-2}T}$
n	Number of bacteria adhered to a surface	[]
n_e	Number of electrons transferred	[]
N_p	Flux of substrate mass in a pipe	$\mathrm{M\,L^{-2}T}$
Q	Total flow rate	$\mathrm{L^3\,s^{-1}}$
Re	Reynolds number, ratio of inertial force to viscous force	[]
Re_p	Reynold's number for a porous media based on the porosity, inertia to viscous forces	[]
S_V	Specific surface area to volume ratio	$\mathrm{L^{-1}}$
Sc	Schmidt number, ratio of particle to momentum diffusivity	[]
Sh	Sherwood number, ratio of total mass transport to diffusive transport	[]
T	Temperature	Θ
U_0	Area averaged velocity	$\mathrm{L\,T^{-1}}$
Z	Complex impedance of solution measured using EIS	Ohm

Chapter 1

Introduction

1.1 Motivation

Organisms respond to stress in different ways. For example, the upper bound on leaf size is determined by water stress [1] while nutrient stress leads to the relaxing of upper bounds on mice and human health.[2, 3] This is complicated by the nature of the stress, whether acute or prolonged. Stress can have far reaching impacts on genetics and/or epigenetics. Microbes are also known to respond to stress. Nutrient stress is known to cause microbes to do everything from decreasing and increasing metabolic rates[4], mass movement of a biofilm [5], abandonment of the safety net of a biofilm,[6] inducing the death of neighboring cells, to forced hibernation. Mechanical stress can also cause many of these same behaviors. Though unlike humans or trees, you cannot ask or run tests on single microbes to examine how stress affects their behavior. The nature of living at the micro-scale changes how we can study them and how they experience stress. Most of the stresses occur in laminar-controlled fluid dynamic regimes and diffusion-controlled mass transport regimes. This limits many studies of microbes to ex vivo measurements or measurements in transparent microfluidic devices. While these studies are useful, they do not translate easily to real-world situations where the laminar and diffusive mass transport is the result of these small cells' ability to exist in the boundary layer of a turbulent or convective dominated bulk flow. We use a system that has been used to systematically translate

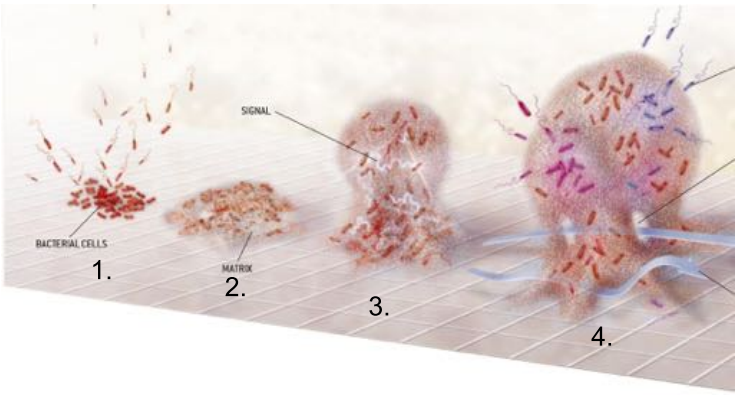

Figure 1-1: Artist rendering of biofilm development. Stage 1 is the initial adhesion of bacteria to the surface, which can include reversible adhesion under flow, the exploration of hammocks and the penetration of solvation layers or hydrophobic air layers. Stage 2: the bacteria in the biofilm start secreting exopolysacchride matrix and reproducing. Stage 3: cell differentiation due to cell signaling. Stage 4: chemical gradients necessitate the creation of fluid channels within the biofilm, dispersion, death and dormancy of cells.[9] Image reproduced from artist rendering of the stages of biofilm development from Costerton and Stewart, 2001. [9]

between scales, a rotating disk electrode. We use the rotating disk electrode to study both adhesion of microbes under hydrodynamic shear and electrical stress and development of those cells into biofilms.

Biofilms are matrix enclosed populations of bacteria adhered to each other, and/or at surfaces and/or interfaces.[7] These structures allow for the biofilm to customize its environment, controlling the pH, substrate flux in and waste flux out. The structures afford resistance to mechanical stress, chemical stress like antibiotics, and predation.[8] For the case of surface bound biofilms, they are initiated by opportunistic bacteria and/or the coating of the surface by environmental proteins, see Figure 1-1.

The initial bacteria are known as anchor cells and serve as the foundation of the biofilm. The bacteria at this stage will start reproducing and attracting new cells by changes in gene transcription and the release of chemotractants.[10, 11] Microbes will then start producing exopolymeric substances that will hold the bacteria together and prevent predation. Within this matrix there are channels for fluid flow and waste removal on the order of $2\,\mu$m in diameter.[12, 13] Biofilms consist of single species

or multiple species working cooperatively.[14] Within biofilms are persister cells that through some yet unknown mechanism resist oxidative and antibiotic stresses and restart the biofilm without any discernible hereditable resistance.[15] Biofilms harvest nutrients from the growth surface of the biofilm or from the surrounding environment. For those harvesting nutrients from the surrounding fluid, there is a conflict of preventing predation by closing itself off from the outside but in order to gain nutrients it would want to be open. For biofilms consuming nutrients from the surface, the challenge is waste removal and exhaustion of the substrate which again requires being open to a potentially hazardous environment. One solution to this challenge is sloughing of the biofilm where a series of chemicals are produced that breakdown the exopolymeric matrix and the bacteria are released into the environment. [16, 17]

Many groundbreaking studies around biofilms were organized around addressing three systems: oral biofilms [7], biofilms for wastewater treatment,[18] and biofouling [19]. Oral biofilms are biofilms that grow on your teeth, gums, and between your gums and teeth. They can cause gum tissue inflammation and tooth decay.[20] These biofilms get their nutrients from the surrounding environment and grow on the surface. A large component of the decay is an unintentional result of waste removal. Biofouling operates in a similar manner. Biofouling occurs when biofilms form on surfaces like ship's hulls and propellors, heat exchangers, and fuel and food pipes.[16] These films create a surface for larger organisms like mollusks and coral to adhere in marine environments. In constrained pipes they cause increased resistance to heat and fluid transport.[16] On metallic surfaces, these biofilms can cause similar decay to teeth by waste products or as an active part of their metabolism.[21, 22] On the other hand, wastewater biofilms are used to treat wastewater by removing organic matter that would result in algal blooms and nitrification of waterways that we return our used water to. Wastewater treatment plants achieve this by flowing the water over rock beds which accumulate biofilms; mixing oxygen with the wastewater and cultures of planktonic bacteria; flowing the wastewater over artificial supports that biofilms grow on; or inducing bacteria to bacteria biofilms. While once viewed as a successor to conventional wastewater treatment, microbial fuel cells, based off of traditional

wastewater treatment designs, show more promise now as a successor tool for studying biofilm dynamics.

Microbial electrochemical cells were considered a key component for bridging the energy/water nexus because of the relationship between water treatment and energy usage.[23, 24, 25] Water treatment accounts for 3% of the total energy consumed in the United States.[26] This level of energy demand is impossible to meet for the developing world producing a global problem since inadequate water treatment leads to disease and death. During the energy crises of the 2000s, it was viewed that the energy problem would be a problem for developed countries as well and that the tradeoff that was extant between aquatic environmental pollution and economic productivity was less attractive.[27] Direct byproducts of wastewater treatment processes include methane gas for fuel and biomass for fertilizer. Other byproducts are sulfur dioxide, silicon dioxide, and ammonia, which unfortunately limit the use of the methane as fuel. Microbial electrochemical cells, which convert chemical energy in wastewater directly to electricity, are a promising alternative to conventional biological wastewater treatment. A microbial fuel cell (MFC) is a type of microbial electrochemical cell where bacteria consume sugars and other hydrocarbons and excrete CO_2, protons and electrons. A typical biofilm formed during operation of an MFC is shown in Figure 1-2a. In an MFC, electrons travel to corrosion resistant metals (the anode) while protons are combined at another electrode (the cathode), with the electrons that have passed through a circuit to generate useful work, Figure 1-2b. Research in the area achieved power densities as high as $1\,\mathrm{kW\,m^{-3}}$ [24] but this may be nearing the limit of power output.[28] While this is still useful for indefinitely powering low-power sensors [29] and providing some power to remote areas, [30] these devices may be more suited to study biofilm processes, bacterial process and cultivating novel bacterial strains. [31, 32]

Not all bacteria can survive in a microbial fuel. To do so, the bacteria, classified as electroactive, must either generate and secrete chemicals that can be oxidized at an electrode surface or directly transfer an electron to the electrode. Those that can do include some of the most widely studied biofilm biofilm forming organisms of the

(a) Scanning electron micrograph of fixed biofilm

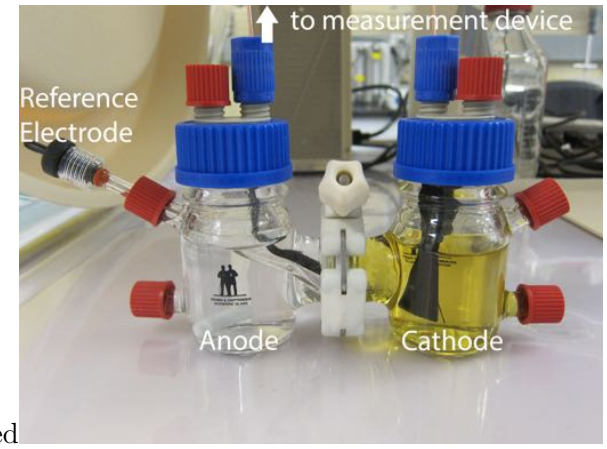

(b) Two chamber microbial fuel cell

Figure 1-2: A Microbial Fuel Cell 1-2b with a *Geobacter sulfurreducens* PCA biofilm 1-2a in the anode and 50 mM ferricyanide in the cathode in our lab.

Pseudomonas spp. It appears that all bacteria are affected by the electrochemical potential of the surface they adhere to. The electrochemical potential of an electrode is one of the many parameters that can optimize microbial fuel cell performance. Furthermore, electroactive biofilms still face many of the challenges that other biofilms do including waste removal, nutrient acquisition, remaining adhered under flow, and preventing predation.

We take these precedents to ask and answer a fundamental question: how does momentum transport affect an electroactive biofilm independently from mass transport? The first answer to the question was made in 1982 [33] but was found inadequate as late as 2006.[34] We show that operating a rotating disk electrode as a microbial electrochemical cell with *Geobacter sulfurreducens* is a platform that can achieve similar answers to systems used in the past with additional benefits of direct, real-time, *in situ* analysis of biofilm response.

1.2 Thesis Overview

In Chapter 2 we demonstrate for the first time that mass transport limiting current, chronoamperometry, and cyclic voltammetry in a rotating disk electrode are favorable for studying adhesion of microbes to metallic surfaces under shear. This is

relevant to the field of microbial biofouling where biofilms adhere to materials involved in liquid transport causing economic loss through corrosion or drag. Microorganisms interacting with surfaces under these open channel flows contend with high shear rates and active transport to the surface. The metallic surfaces they interact with carry charge at various potentials that are little addressed in literature. We study the adhesion of *Escherichia coli*, *Bacillus subtilis*, and 1 μm silica microspheres over a range of shear stresses. Our results agree with literature on red blood cells in rotating disk electrodes and deposition rates of *B. subtilis* and *E. coli* from optical systems, and show that we can quantify changes in active electrode area by bacteria adhesion and protein secretion. Our methodology measures changes in area instead of mass simultaneously providing measurements of the protein binding step that initiates biofilm formation. Unlike fluorescence microscopy, these methods are in vivo and apply to a larger range of problems than on-chip flow devices.

In Chapter 3 we use the rotating disk system to present the first study of how electroactive biofilms adapt to shear stress over time. These biofilms are unique in that they do not rely on electron acceptor diffusion as they are "wired" to the electron acceptor, leading to thicker biofilms. Furthermore, it is possible to use the current produced by the biofilms as a proxy for metabolic respiration. We measure current, open circuit potential, electron diffusion current, electrochemical impedance, and formal potential throughout the course of seven days of *Geobacter sulfurreducens* forming a biofilm on a graphite disk exposed to three different shear stresses (1, 0.1, 0.01 Pa) and fixed mass flux. We image the resulting biofilm to measure biofilm thickness, porosity, and surface roughness. We find that high shear rates lead to faster start-up times and higher current, and by proxy higher metabolic rates, at the cost of long term sustainability of this current. We also find that there was no statistical difference in thickness or surface roughness between biofilms of different stresses. Similar to previous work, we propose that the lack of stability is due to the absence of waste removal.

References

[1] Kaare H Jensen and Maciej A Zwieniecki. Physical limits to leaf size in tall trees. Physical Review Letters, 110(1):018104, 2013.

[2] Y-H Yu, JR Vasselli, JR Vasselli, Y Zhang, JI Mechanick, JI Mechanick, J Korner, J Korner, R Peterli, and R Peterli. Metabolic vs. hedonic obesity: a conceptual distinction and its clinical implications. Obesity reviews : an official journal of the International Association for the Study of Obesity, 16(3):234–247, 2015.

[3] Danielle Naville, Claudie Pinteur, Nathalie Vega, Yoan Menade, Michèle Vigier, Alexandre Bourdais, Emmanuel Labaronne, Cyrille Debard, Luquain-Costaz, Céline, Martine Bégeot, Hubert Vidal, and Magueresse-Battistoni, Brigitte. Low-dose food contaminants trigger sex-specific, hepatic metabolic changes in the progeny of obese mice. The FASEB Journal, 27(9):3860–3870, 2013.

[4] Susmita Sahoo, Rajesh K Verma, AK Suresh, Krishnamurthy K Rao, Jayesh Bellare, and GK Suraishkumar. Macro level and genetic level responses of bacillus subtilis to shear stress. Biotechnology Progress, 19(6):1689–1696, 2003.

[5] Haiyang Zhang, Zalman Vaksman, Douglas Litwin, Peng Shi, Heidi Kaplan, and Oleg Igoshin. The mechanistic basis of *Myxococcus xanthus* rippling behavior and its physiological role during predation. PLoS Comput Biol, 8(9):e1002715, 2012.

[6] Ymele-Leki, P and JM Ross. Erosion from staphylococcus aureus biofilms grown under physiologically relevant fluid shear forces yields bacterial cells with reduced avidity to collagen. Applied and environmental microbiology, 2007.

[7] William J Costerton, Zbigniew Lewandowski, Douglas E Caldwell, Darren R Korber, and Lappin-Scott, Hilary M. Microbial biofilms. Annual Reviews in Microbiology, 49(1):711–745, 1995.

[8] Brandon W Peterson, Yan He, Yijin Ren, Aidan Zerdoum, Matthew R Libera, Prashant K Sharma, Arie-Jan van Winkelhoff, Danielle Neut, Paul Stoodley, Henny C van der Mei, and Henk J Busscher. Viscoelasticity of biofilms and their recalcitrance to mechanical and chemical challenges. Fems Microbiol Rev, 39(2):234–245, 2015.

[9] JW Costerton and Philip S Stewart. Battling biofilms. Sci Am, 285(1):74–81, 2001.

[10] AP Annachhatre and SMR Bhamidimarri. Microbial attachment and growth in fixed-film reactors: Process startup considerations. Biotechnology Advances, 10(1):69–91, 1992.

[11] Hall-Stoodley, Luanne, William J Costerton, and Paul Stoodley. Bacterial biofilms: from the natural environment to infectious diseases. Nat Rev Microbiol, 2(2):95–108, 2004.

[12] Paul Stoodley, Dirk deBeer, and Zbigniew Lewandowski. Liquid flow in biofilm systems. Appl Environ Microbiol, 60(8):2711–2716, 1994.

[13] Paul Stoodley, John D Boyle, Dirk deBeer, and Lappin-Scott, Hilary M. Evolving perspectives of biofilm structure. Biofouling, 14(1):75–90, 1999.

[14] Carey D Nadell, Joao de Xavier, and Kevin R Foster. The sociobiology of biofilms. FEMS microbiology reviews, 33(1):206–224, 2009.

[15] Kim Lewis. Persister cells. Microbiology+, 64(1):357–372, 2010.

[16] Michael Trulear and William G Characklis. Dynamics of biofilm processes. Journal (Water Pollution Control Federation), 54(9):1288–1301, 1982.

[17] Ursula Telgmann, Harald Horn, and Eberhard Morgenroth. Influence of growth history on sloughing and erosion from biofilms. Water Research, 38(17):3671–3684, 2004.

[18] Bruce E Rittmann and McCarty, Perry L. Model of steady-state-biofilm kinetics. Biotechnology and Bioengineering, 22(11):2343–2357, 1980.

[19] Gregory Bixler and Bharat Bhushan. Biofouling: lessons from nature. Philosophical Transactions Royal Soc Lond Math Phys Eng Sci, 370(1967):2381–2417, 2012.

[20] Laurence J Walsh. Dental plaque fermentation and its role in caries risk assessment. International Dentistry SA, 8(5):34–40, 2006.

[21] DJ Schiffrin and De SR Sanchez. The effect of pollutants and bacterial microfouling on the corrosion of copper base alloys in seawater. Corrosion, 41(1):31–38, 1985.

[22] HP Volkland, H Harms, Oskar Wanner, and AJB Zehnder. Corrosion protection by anaerobiosis. CLEAN – Soil, Air, Water, 44(8):103–106, 2001.

[23] Bruce E Logan and John M Regan. Electricity-producing bacterial communities in microbial fuel cells. Trends in Microbiology, 14(12):512–518, 2006.

[24] Bruce E Logan. Scaling up microbial fuel cells and other bioelectrochemical systems. Applied Microbiology and Biotechnology, 85(6):1665–1671, 2009.

[25] Bruce E Logan and Korneel Rabaey. Conversion of wastes into bioelectricity and chemicals by using microbial electrochemical technologies. Science, 337(6095):686–690, 2012. 10.1126/science.1217412.

[26] Water & sustainability (Volume 4): U.S. electricity consumption for water supply & treatment - the next half century. Technical Report 1006787, EPRI, Palo Alto, CA, 2002.

[27] Eloise M Biggs, Eleanor Bruce, Bryan Boruff, John MA Duncan, Julia Horsley, Natasha Pauli, McNeill, Kellie, Andreas Neef, Floris Ogtrop, Jayne Curnow, Billy Haworth, Stephanie Duce, and Yukihiro Imanari. Sustainable development

and the water–energy–food nexus: A perspective on livelihoods. Environmental Science and Policy, 54:389–397, 2015.

[28] Sudeep C Popat and César I Torres. Critical transport rates that limit the performance of microbial electrochemistry technologies. Bioresource Technology, 215:265–273, 2016.

[29] Jan BA Arends. The next step towards usable microbial bioelectrochemical sensors? Microbial Biotechnology, 2017.

[30] Folusho F Ajayi and Peter Weigele. A terracotta bio-battery. Bioresource Technology, 116:86–91, 2012.

[31] Colin Wardman, Kelly P Nevin, and Derek R Lovley. Real-time monitoring of subsurface microbial metabolism with graphite electrodes. Front Microbiol, 5:621, 2014.

[32] Hend MM Selim, Ahmed M Kamal, Dina MM Ali, and Rabeay YA Hassan. Bioelectrochemical systems for measuring microbial cellular functions. Electroanal, 2017.

[33] Bruce E Rittman. The effect of shear stress on biofilm loss rate. Biotechnology and Bioengineering, 24(2):501–506, 1982.

[34] I.W.A.T.G.B. Modeling. Mathematical Modeling of Biofilms. Scientific and Technical Report Series. IWA Publishing, 2006.

Chapter 2

In situ quantification of bacterial adhesion to electrically polarized metallic surfaces under shear

2.1 Introduction

In oil pipelines, food production systems, and on ship's hulls and propellers, adhering bacteria experience significant shear stress. Bacterial adhesion is not only a matter of the relative surface energies of the material and bacterium, but also of the flow conditions, substrate (food) concentration, and surface charge of the material.[1, 2] Bacteria adhered to surfaces display a completely different phenotype compared to when bacteria are suspended.[3, 4] There is extensive work on bacterial adhesion in relation to biofouling of implanted medical devices and the materials used therein, however, the extent of that work on metals under non-medical situations is limited.[5] These non-medical economically relevant conditions include losses of $\sim$ \$56 billion annually due to biofouling of US Navy ship hulls and significant losses in both oil and food distribution.[6, 7, 8] These scenarios are more suitable for investigation using rotating disk systems than channel flow cells where mass flux is coupled to shear stress and sedimentation is the primary mechanism of cell-surface interaction.[3, 9]

Rotating disk systems have been used to study mass and momentum transport phenomena because of the analytic approximations for surface flux, well controlled experimental variables, and the ease of relating results from this system to practical systems such as pipes and flat plates. For example, the rotating disk environment has also been used to mimic flow conditions in blood vessels.[10] Adhesion of platelets, *Staphylococcus* spp., and migration and adhesion of leukocytes were studied in rotating disk systems quantifying adhesion after the fact with fluorescence microscopy.[11, 12] The binding of albumin proteins to implanted medical devices was studied using the change in electrochemical impedance as a proxy for platelet binding. [10]

Rotating Disk Electrodes (RDEs) are used to study reactions on planar electrodes in a highly conductive medium ($> 1\ \mathrm{S \cdot cm^{-1}}$) with a minimal number of supporting electrolytes.[13] These electrochemical reactors are designed to minimize noise from factors not related to the reactions being studied such as edge effects, other species, concentration and temperature fluctuations.[14] Care needs to be taken when using these systems to study bacteria because these design constraints are violated therein. For example, when RDEs are used to study microbial induced corrosion or conductive biofilms, fresh or seawater medium is used, which have a low conductivity ($\sim 1\ \mathrm{mS \cdot cm^{-1}}$) multicomponent mixture of ions.[15, 16, 17, 18] Furthermore, the presence of bacteria may introduce unaccounted for noise into standard methods. For example, it is well established that CuO, ZnO, Al_2O_3, SiO_2, latex nanoparticles (30 – 50 nm) and microparticles (3 – 11 μm) enhance mass transfer to the rotating disk.[18, 19, 20] On the other hand, normal red blood cells in isotonic solutions decrease the mass transport more than glutaraldhyde fixed (inflexible) red blood cells and 9 μm alumina particles in the same solution.[21, 22]

Microbial adhesion has not been studied when rotating disk electrode systems are used to study microbial electrochemical systems and microbial induced corrosion.[17, 23, 24] Studies on adhesion and attraction of platelets, *Staphylococcus* spp., and white blood cells in rotating disk systems did not leverage the electrochemical origins of this technique.[11, 12] The purpose of the present study is to use the suite of electrochem-

ical methods designed for an RDE to study bacteria as they transition from their planktonic to biofilm state. Furthermore, the point at which shear-induced adhesion is initiated is determined using electrochemical methods. We address concerns of how biological media and particles of similar size to bacteria may impact diffusivity, viscosity, and conductivity within these measurements. This finding is applied to monitor the adhesion of bacteria at a fixed electrode potential and shear rate.

2.2 Methods

We use an RDE to quantitatively measure the adhesion of bacteria and bacterial proteins using electrochemical methods. Ficquelmont-Loizos et al., described 13 parameters that can impact electrochemical measurements in rotating disk electrodes: particle nature (e.g. bulk averaged electrostatic interaction energy, surface roughness, asymmetry, stiffness, charge, etc), density, volume concentration, size, size distribution; medium nature (the solvent), temperature, viscosity, conductivity; and the electrode rotation rate, type, diameter, and roughness.[19] We hold all the parameters constant except the particle composition and their subsequent properties, electrode roughness, and rotation rate.

2.2.1 Materials

The media is 4.33 g Na_2HPO_4, 2.69 g NaH_2PO_4, 0.31 g NH_4Cl, 0.13 g KCl, (MilliporeSigma, Darmstadt, GER) in 1 L of deionized water, similar to what has been used in previous bioelectrochemistry experiments.[25] This media is amended with 3.9% glycerol to be isotonic with the bacterial growth media. The resulting conductivity is 4.91 $mS \cdot cm^{-1}$ at 30 °C. The density of the media is $1.01 \pm 0.01\,g \cdot cm^{-3}$ at 30 °C. The viscosity of the amended media is $0.00145 \pm 0.00003\,Pa\,s$ without particles. Subsequent viscosity with particles is measured at shear rates of $100 - 1000\,s^{-1}$ at 30 °C using a 60 mm diameter 2° steel cone with solvent trap on a water cooled Peltier plate (AR-G2, Waters Corporation, New Castle, DE, USA). The redox couple used

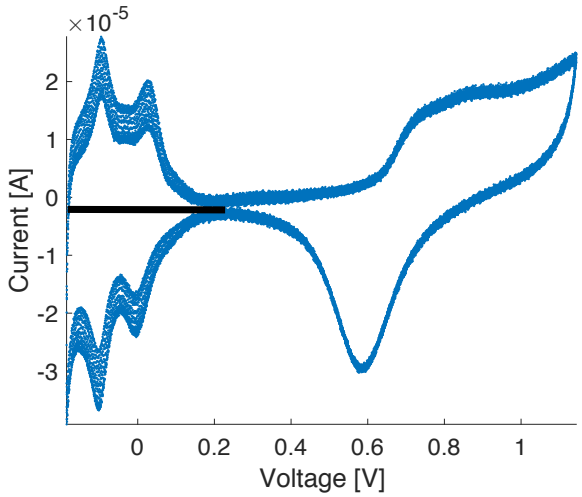

Figure 2-1: Sample cyclic voltammogram of the bare electrode between experiments. Between each experiment the electrodes were prepared by; (1) rinsing in 1 N sodium hydroxide solution at 2000 rpm, (2) poising the electrode at 2 V vs SHE and, (3) performing cyclic voltammetry eight times in 1 N sulfuric acid. The electroactive area was estimated by integrating under the solid black line shown on the graph and dividing by the area that a hydrogen molecule can occupy on a platinum surface.

for electrochemical methods is the quasi-reversible ferri/ferrocyanide couple

$$\mathrm{Fe(CN)_6}^{4+} + \mathrm{e}^- \rightleftharpoons \mathrm{Fe(CN)_6}^{3+}, 0.358\ \mathrm{V\ vs\ SHE} \tag{2.1}$$

[26] diluted to 10 mM from a 1 M ferricyanide stock solution (MilliporeSigma, Darmstadt, GER). The potential in the chosen media at 30 °C is 0.192±0.011 V vs Ag/AgCl (3.8 M KCl) or 0.394 ± 0.011 V vs SHE.

2.2.2 Apparatus

A 0.4 cm diameter platinum working electrode (Pine Instruments, Durham, NC, USA) is used as the working electrode. The electrode is soaked in 1 M sodium hydroxide at 2000 rpm for 15 minutes to rinse off ferrocyanide between experiments. Next, the electrode is cleaned and the electroactive area of the platinum electrode is calculated following the method of Woods, 1974 (see Figure 2-1).[27] In brief, the electrode is poised in 1 M sulfuric acid at 2.044 V vs Ag/AgCl (3.8 M KCl)

for 1 min at 2500 rpm. Cyclic voltammetry is performed on the working electrode from -0.186 – 1.144 V vs Ag/AgCl (3.8 M KCl) at 50 $mV \cdot s^{-1}$ for 8 cycles. These two steps are repeated until the electroactive area is approximately equal to that of the previous experiment $\sim$ 0.3 cm^2 for the smooth electrode and $\sim$ 0.5 cm^2 for the roughened electrode (see Figure 2-1). The electrode is initially polished using 6, 0.5, and 0.1 μm diamond polishing paste (TedPella, Redding, CA, USA). When roughened, the electrode is treated using 5 μm grit silicon carbide polishing paper. A single junction Ag/AgCl (3.8 M KCl) reference electrode (MilliporeSigma, Darmstadt, GER) is used because the conductivity of the media is too low to sustain a double-junction. A 0.1 cm diameter coiled platinum wire electrode behind a glass frit is used as the counter electrode (Pine Instruments, Durham, NC, USA).

The reactor is a water jacketed inverted 500 mL Erlenmeyer flask, with four ports for electrodes and gas (Pine Instruments, Durham, NC, USA). The reactor is maintained at a constant temperature of 30 °C using a water jacket (Julabo E5, Julabo USA, Allentown, PA, USA). The system is purged and blanketed at 50 sccm with ultra-high purity nitrogen gas (Airgas Inc, Radnor Twp, PA, USA). The current is measured with a Gamry Reference 600 (Gamry Instruments, Philadelphia, PA, USA) with a resolution of 600 mA and a bandwidth of 10 MHz, which is much lower than the sampling rate and current measured.

2.2.3 Cells and Particles

We use the model gram-negative bacterium, *Escherichia coli* K12 CGSC 4401, and the model gram-positive, biofilm forming organism, *Bacillus subtilis* BGSC 1A1. Bacteria stiffness differs from previously tested particles and can range from 50 – 200 MPa, the lower range being gram-negative and the higher range being gram-positive.[28] *E. coli* and *B. subtilis* are commonly used in bacterial studies for their relevance in biochemical production, and both have well characterized material and physiological properties. Each is grown in two 125 mL flasks containing 50 mL Luria-Bertani media (Becton, Dickinson and Co, Franklin Lakes, NJ, USA) at 37 °C in shaking incubators at 250 rpm. After reaching mid-log phase (4 hrs for *E. coli*,

Table 2.1: Size and length are comparable to those found by Bronk et al.,[30] while beads measurements are based on manufactures label (Spherotech, Inc, Lake Forest, IL, USA)

Particle	OD600	volume fraction [%]	Density [$g \cdot cm^3$]	Length [μm]	Diameter [μm]
Media			1.01 ± 0.01		
Beads	2.34 ± 0.01	5.8 ± 0.0	1.03 ± 0.00		1.04
E. coli	0.73 ± 0.06	0.26 ± 0.02	1.02 ± 0.01	3.33 ± 0.54	0.85 ± 0.17
B. subtilis	0.63 ± 0.22	0.08 ± 0.03	1.03 ± 0.01	7.10 ± 1.23	0.99 ± 0.22
E. coli roughened electrode	0.72 ± 0.18	0.25 ± 0.06	1.03 ± 0.01	3.33 ± 0.54	0.85 ± 0.17
B. subtilis roughened electrode	0.85 ± 0.06	0.11 ± 0.01	1.03 ± 0.01	7.10 ± 1.23	0.99 ± 0.22

4.5 hrs, *B. subtilis*), the cells are centrifuged twice at 5000 rpm for 10 min and rinsed in between with the media described earlier. Optical density is measured at 600 nm following standard methods [29] (UV-1800, Shimadzu, Nakagyo-ku, Kyoto, JPN) after suspending the cells in the full 100 mL. Cell density is calculated using a disposable hemocytometer (Incyto, Co., Ltd, Chonan-si, Chungnam-do, KOR). Cell volume is calculated assuming the bacteria are cylindrical and measuring them was achieved using a 100 X oil immersion objective. Cell death is qualitatively measured for *E. coli* and *B. subtilis* by comparing streaks on LB agar before and after each experiment. Polystyrene spherical beads 1.04 μm in diameter are used as a control (Spherotech, Inc, Lake Forest, IL, USA). The beads are vortexed in 70% ethanol before centrifugation for 10 minutes at 12000 rpm, then rinsed with DI water, prior to being suspended in the test media and sonicated. The beads are supplied at a stock concentration of 5% w/v with a density of 1.96 $g \cdot mL^{-1}$ or equivalently a volume fraction of $\phi = 2.04\%$ v/v. The properties of the media and suspensions are described in Table 2.1.

2.2.4 Reactor operation

The media is brought to 30 °C from 20 °C in $\sim$ 15 s and deoxygenated using nitrogen for 15 minutes at 1000 rpm.[31] The bacteria are streaked on LB agar plates after suspending the bacteria in the RDE in 100 mL of the media and incubated at 37 °C. The suspension is weighed and measured in 1 mL samples after the cells or particles have been mixed. A volume of 1 mL of 1 M ferricyanide replaces the 1 mL of suspended bacteria. Internal resistance of the media is 128(14) Ω. To determine the onset of adhesion, a Levich curve is created by linear sweep voltammetry (LSV) from 350 mV to -350 mV vs Ag/AgCl (3.8 M KCl) at 50 $mV \cdot s^{-1}$ and 2 mV per step over the rotation range of 50 – 2000 rpm, 50 rpm per step. These rotation rates are equivalent to shear stress of 0.15 – 37.33 $dynes \cdot cm^{-2}$ and shear rates of 14.73 – 3727.28 s^{-1} and almost covers the entire range of practical scenarios highlighted.[32] Three cycles of cyclic voltammetry are taken before and after the LSV from 650 to -250 mV vs Ag/AgCl (3.8 M KCl) at 200 $mV \cdot s^{-1}$ to verify that adhesion occurred. We sweep backwards along rotation rates to check for hysteresis. Each experiment takes 3 hrs from the time the bacteria are removed from their growth media until they are plated a second time. The buffer experiment took 4.5 hrs because an electrochemical impedance spectrum is used to find the diffusivity of the redox couple according to Tribollet et al., 1988 (see Figure 2-2a and 2-2b).[33] All conditions are run in triplicate.

2.3 Results and Discussion

We use an RDE to study the adhesion of bacteria under shear at a charged surface. We first characterize the rotating disk system noting that the media we use is not a single, highly conductive, electrolyte solution. The diffusivity of ferricyanide is $1.55 \pm 0.18 \times 10^{-5}$ $cm^2 \cdot s^{-1}$ in the chosen buffer media at 30 °C (see Figure 2-2a and 2-2b). This is greater than the 0.834×10^{-5} $cm^2 \cdot s^{-1}$ in 1 M potassium chloride and 500 ppm polyethylene oxide at 28 °C or the 0.77×10^{-5} $cm^2 \cdot s^{-1}$ in 1 M potassium chloride at 25 °C.[34, 35] The product of diffusivity and viscosity over temperature is

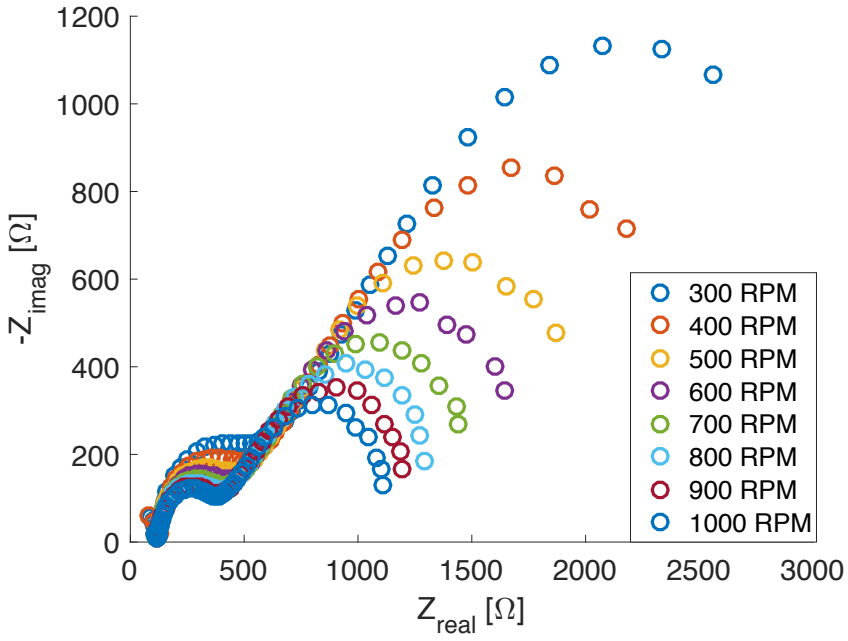

(a) Raw EIS

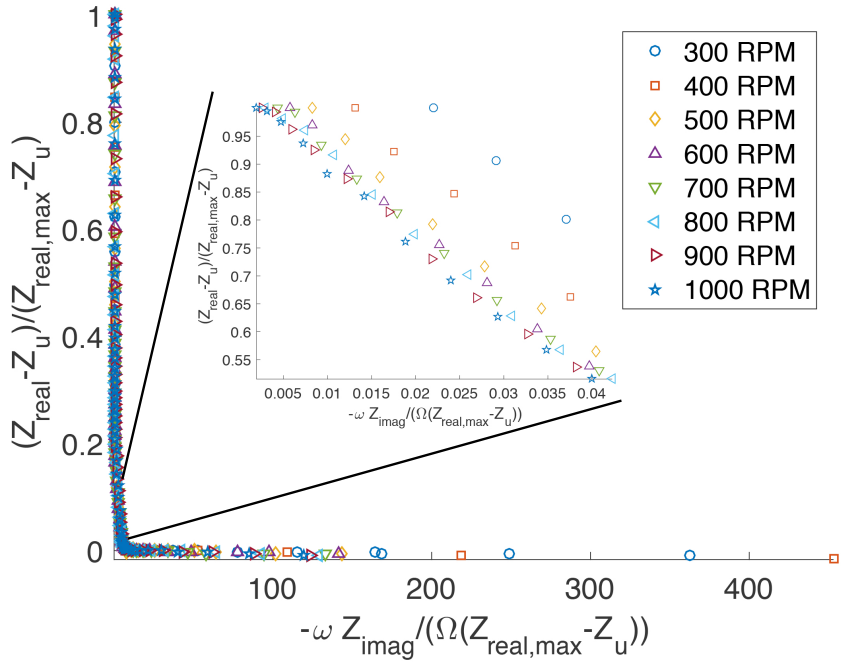

(b) Tribollet's Dimensionless EIS

Figure 2-2: Electrochemical impedance spectrum to determine diffusivity Figure 2-2a. Using the method of Tribollet et al., [33] the slope of the dimensionless line, Figure 2-2b inset, can be used to calculate the diffusivity of the redox tracer used. Ferricyanide diffusivity is calculated to be $1.55(18) \times 10^{-5}\,\mathrm{cm}^2 \cdot \mathrm{s}^{-1}$ at 30 °C in a phosphate buffer solution amended with 30% glycerol. This is greater than the diffusivity in 1 M potassium chloride solutions, but follows the trend for higher glycerol concentrations. The experiments were performed in technical triplicate.

the Einstein-Stokes ratio, Equation 2.2,

$$\frac{D_0 \mu}{T} \tag{2.2}$$

and is one way to compare diffusivities across different media with different viscosities at slightly different temperatures. For polyethylene oxide concentrations of 500 ppm and 1000 ppm the Einstein-Stokes ratio is 3.387×10^{-10} g $\cdot$ cm $\cdot$ s^{-2} $\cdot$ K^{-1} and 3.816×10^{-10} g $\cdot$ cm $\cdot$ s^{-2} $\cdot$ K^{-1} at 28 °C and 30.4 °C respectively. The Einstein-Stokes ratio is 2.2×10^{-10} g $\cdot$ cm $\cdot$ s^{-2} $\cdot$ K^{-1} in 1 M potassium chloride with no polyethylene. Based on the trend seen with polyethylene, we conclude the higher value of the Einstein-Stokes ratio of 7.7×10^{-10} g $\cdot$ cm $\cdot$ s^{-2} $\cdot$ K^{-1} in our work is due to the 3.5 % or 35000 ppm glycerol concentration.

We explore four hypotheses for the observed deviation from the Levich curve in Figure 2-4: (1) viscosity changes caused by the presence of particles or live bacteria; (2) enhanced mass transport from flexible particles; (3) changes in media conductivity from the death of bacteria; and (4) changes in concentration due to metabolic consumption of the tracer chemical. The viscosity and the density of the solution does not vary significantly with the particles concentrations used, as shown in Figure 2-3. *B. subtilis* concentrations were $\sim$ 0.10 %v/v and *E. coli* concentrations were $\sim$ 0.25 %v/v. We assume Batchelor's[36] 2nd order correction for viscosity with particles for the volume fractions $\phi < 5\%$,

$$\mu^* = \mu \left(1 + \frac{5}{2}\phi + 7.6\phi^2\right). \tag{2.3}$$

Equation 2.3 and Einstein's 1$^{\text{st}}$ order approximation that it reduces to are not accurate for volume fractions 1 – 10% but are widely used in the literature up to that limit.[37] We also use Equation 2.3 to normalize across the various volume fractions between our samples and those explored in the literature. We create a modified Sherwood

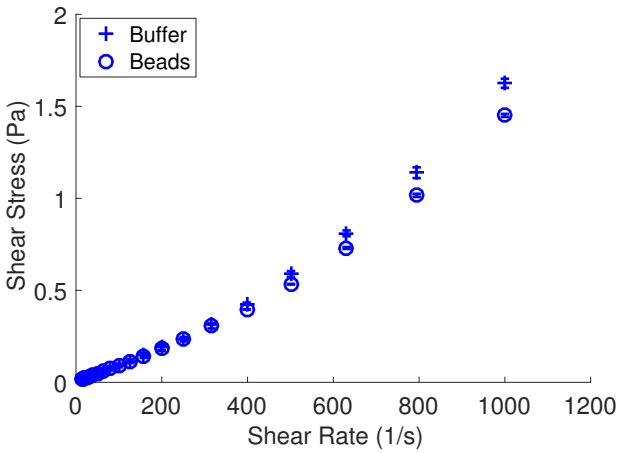

Figure 2-3: Rheological data. The slope of shear stress versus shear rate is the viscosity of the solution with given particles. Each rheological experiment took an hour and the viscosity did not change over this time. The absence of the change in viscosity with each particle has been seen in literature for particle concentrations this low.

number using the modified viscosity in the Reynolds number, as

$$\mathrm{Sh}^* = \mathrm{Sh} \cdot \left(1 + \frac{5}{2}\phi + 7.6\phi^2\right)^{1/2} \mathrm{Sc}^{-1/3} = \mathrm{Re}^{1/2} \tag{2.4}$$

As expected, we find that the reaction of ferricyanide in the abiotic buffer maintains an approximate 1/2 power dependence between Sh and Re, as shown in Figure 2-4 and predicted by Equation 2.4. We assume a 1/2 power slope dependence and plot a line using an intercept from a linear best fit to the data. The intercepts of the lines deviate significantly because the bulk of the points are after the inflection. The slopes for the buffer in the smooth ($S_a = 2.5$) and rough ($S_a = 3.9$) cases are 0.45, but there is curvature in both the *E. coli* and *B. subtilis* cases. The rest of the results presented explore this curvature. The addition of particles can have an impact on mass transport in general and mass transport limiting current in particular, represented by the Levich curve, as shown in the literature for high concentrations of inert nanoparticles and macroparticles. We use 1.04 μm diameter polystyrene beads at a volume concentration of $\sim 5\%$ v/v average to the buffer and the experimental results differed distinctly from those of the *E. coli* and *B. subtilis*. In contrast to similar work

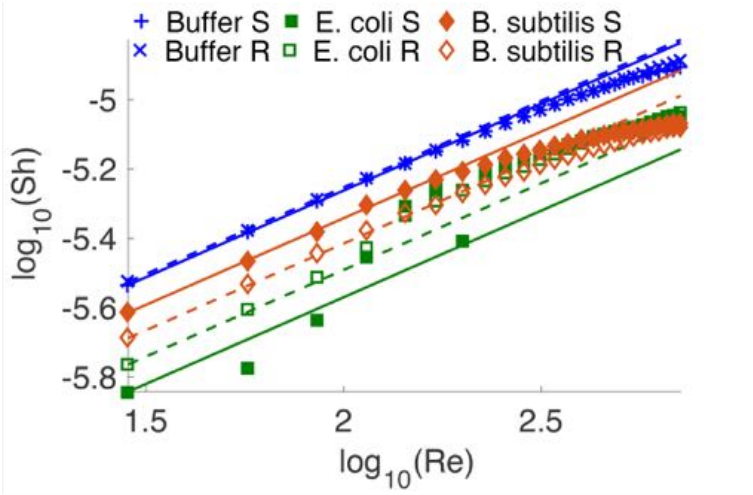

Figure 2-4: Log scale plot of the modified Sherwood number vs Reynolds number for buffer media used in all experiments, *E. coli* K12 CGSC 4401; *B. subtilis* 168 BGSC 1A1 on smooth 'S' and roughened 'R' electrodes. The Sherwood number is modified by the particle concentration according to Batchelor, as shown in Equation 2.4.[36] The relationship between this mass transport number versus the momentum transport number is theoretically predicted to be a power law to the 1/2, as shown in Equation 2.4. Decreased slopes indicate impedance to mass transport whereas increased slopes indicate enhancement. Similar deviation from this power law has been seen in red blood cells at similar concentrations and higher Reynolds numbers (cf. Caprani et al.,[38] and Figure 2-5). Deviation at lower Reynolds numbers has been shown for higher concentrations of inert particles. The data presented is an average of three biological replicates. For clarity, error bars are presented in a linear plot in SI Figure 4.

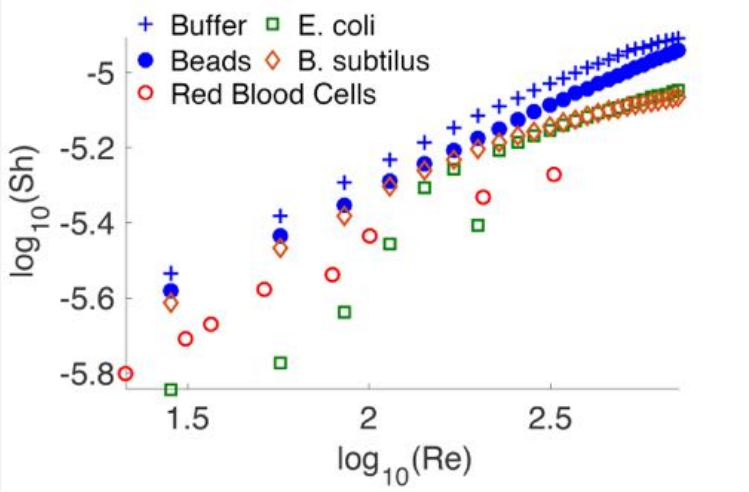

Figure 2-5: Comparison with red blood cells from Caprani et al.,[38] on smooth electrodes. The deviation from a straight line with red blood cells in an isotonic KCl solution was shown as an impedance to mass transport by Caprani et al.,[38] at high Reynolds numbers and explained by adhesion of the cells to the electrode surface. Their data extends to Re = 3000 due to a larger electrode area. The values of tracer diffusivity and viscosity of the isotonic KCl solution used in Caprani et al., were not reported so we use diffusivity of 1.90 $cm^2 \cdot s^{-1}$ and viscosity of 0.00903 P of isotonic KCl at 25 °C from other literature.[19, 40]

by Meinders et al.,[39] which showed that 0.736 μm polystyrene particles adhered to glass at rates similar to those of bacteria, we do not see evidence of adhesion of our 1.04 μm polystyrene particles. This is likely due to the shear rates in this experiment being much higher than the 50 s^{-1} used in theirs. Furthermore, our flow geometry is more applicable to practical systems that rely on forced convection to and away from the surface similar to propellers and the upper walls of pipes. A similar deviation to our work was demonstrated for the adhesion of red blood cells by Caprani et al.,[19] and is shown in Figure 2-5. Our results are inconsistent with studies showing a decrease in viscosity with high concentrations of *E. coli*,[41] since this would lead to an increase in current, from the Levich equation (Equation A.19). For *E. coli* there is an overall decrease in mass transport, not an increase, as shown with nanoparticles.[42] Compared to bacteria, beads should have similar hydrodynamic effects based on size and volumetric density.[43] The stiffness of bacteria differs significantly from beads, the membrane is stiffer and more rigid than the intracellular contents leads them to

Figure 2-6: At 600 rpm before and after a 2 hr exposure to shear stress *E. coli* and *B. subtilis* were streaked on agar plates and incubated at 30 °C.

behave as semi-flexible rods. This was partially tested in Caprani et al.,[38] with glutaraldehyde fixed and non-fixed red blood cells where the fixed cells yielded a Levich curve identical to solid particles. Since *B. subtilis* has a stiffer cell membrane than *E. coli*, 50 – 150 MPa vs 100 – 200 MPa, the results of this work show stiffness may not be the cause of this effect because *B. subtilis* deviates further from the Levich curve than *E. coli*.[38, 28] Cell death would lead to an increase in conductivity and current, not seen in this deviation. Furthermore, plating shows no substantial decrease in cell counts Figure 2-6. An additional cause for the deviation between the Levich curve and those found with live bacteria in this work or live red blood cells in Caprani et al., may be that metabolic consumption or absorption of the reactant ($FeCN_{63}^{+}$ or O_2) by the *E. coli* or red blood cells RBCs respectively. This would be equivalent

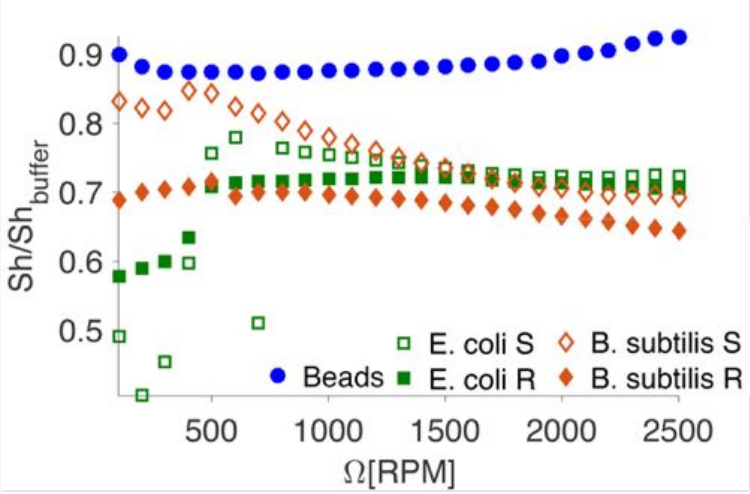

Figure 2-7: The ratio of the particle Sherwood number to the buffer Sherwood number. As shown in Equation 2.4 the ratio of Sherwood number should be constant. Rheological measurements show that viscosity typically does not change upon addition of such a small number of particles, live or dead (Figure 2-3 and Ryan et al.,[47]). The diffusivity would not be expected to appreciably change according to the model developed by Tribollet et al.[33] Since the ratio of particle to buffer Sherwood number is stable for the beads, we can assume that the deviation from the Levich dependence is not due to Coulombic reactions of ferri/ferrocyanide or pure hydrodynamics. *E. coli* can metabolize 5% of the ferricyanide in solution over the 2 hr experiment if they also had an electron donor.[45] The only variable unaccounted for in the Levich equation is the area. The results show an inflection point in the change in area around 600 rpm for *E. coli* and 500 rpm for *B. subtilis*.

to lowering c_∞ in Equation A.19. Red blood cells absorb O_2, with $t_{1/2} = 89$ ms.[44] The time was not mentioned in Caprani et al.,[38] so it is difficult to estimate the effect. *E. coli* has a specific ferricyanide reduction rate of 43 μmol $\cdot$ min^{-1} $\cdot$ g^{-1} under anaerobic conditions with no substrate.[45] The Levich curve takes 55 min to complete, the dry weight of the *E. coli* is $\sim$ 0.025 g results in 0.05 mmol ferricyanide consumed, which is much less than the 1 mmol present in solution. Furthermore, there is very little shift between the forward and backwards curves for our live *E. coli* and *B. subtilis* so that if consumption was occurring, it is not impacting current. It is possible for *B. subtilis* to utilize ferricyanide but there are no consumption rates documented to the authors' knowledge.[46] Linear data makes determining an inflection point of sufficient magnitude in the Levich curve using numerical methods

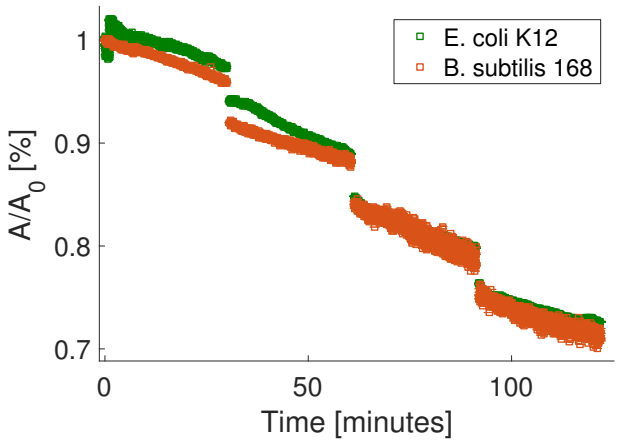

Figure 2-8: Ratio of surface area over initial surface area at a fixed rotation rate. At 600 rpm, (613.02 s^{-1}, 6.14 dynes $\cdot$ cm^{-2}), we measured current over two hours for three biological replicates. The mean and standard deviation are shown. The ratio of measured current to initial current should remain steady since the concentration, viscosity and diffusivity do not change appreciably over this range. According to Equation A.19, the only remaining variable is the area.

difficult. However, by plotting the ratios of the Sherwood number for each particle to that of the buffer solution it is possible to determine the rotation rate that leads to the deviation from linear behavior. As shown in Figure 2-7, it is clear that there is an inflection point around a rotation rate of 600 rpm (613.02 s^{-1}, 6.14 dynes $\cdot$ cm^{-2}) for bacteria but not for the beads. Chronoamperometry was run for 2 hrs at this rotation at limiting current to determine if limiting current can dynamically measure a change in area over time. As shown in Figure 2-8, the ratio of measured current with bacteria to the initial current of the buffer falls over this time. Each break in the data is a cyclic voltammetry measurement. Cyclic voltammetry describes changes in the electroactive area of a surface for a redox molecule. The smaller the enclosed area of the voltammogram, the smaller the electroactive area, as we see for *E. coli* in Figure 2-9.[13] Quantitative analysis requires knowing the mechanisms of attachment and detachment of the redox molecule on the material used.[27] In the present case, the mechanisms of ferricyanide/ferrocyanide reacting on platinum have not been reported in the literature. Recognizing that the area in Equation A.19 is the surface area and not the electroactive area, the change in the limiting current shown in Figures 2-4,

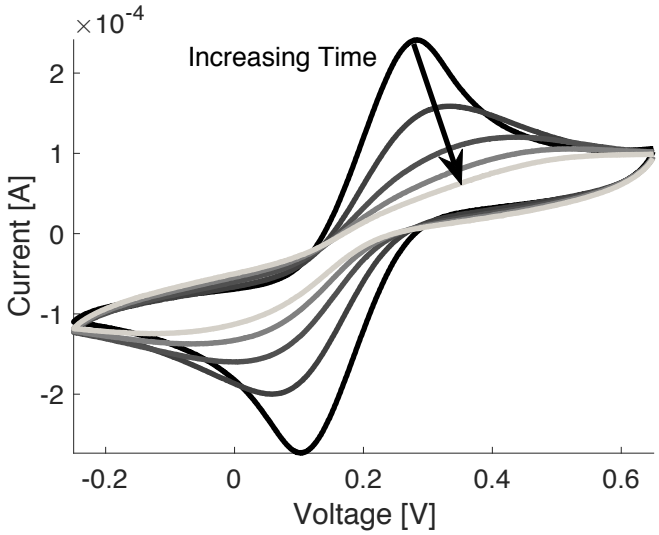

Figure 2-9: Sample cyclic voltammogram over time. Cyclic voltammetry describes changes in the electroactive area of a surface for a redox molecule.[13] The smaller the enclosed area in the voltammogram, the smaller the electroactive area. Quantitative analysis requires knowing the mechanisms of attachment and detachment of the redox molecule on the material used.[27] In the present case, ferricyanide/ferrocyanide reacts on platinum, but the mechanisms of ferricyanide/ferrocyanide have not been reported in the literature and are beyond the scope of this work. Each voltammogram was taken every 30 min at 200 $\mathrm{mV} \cdot \mathrm{s}^{-1}$. A representative cyclic voltammogram for *E. coli* K12 CGSC 4401 is shown here.

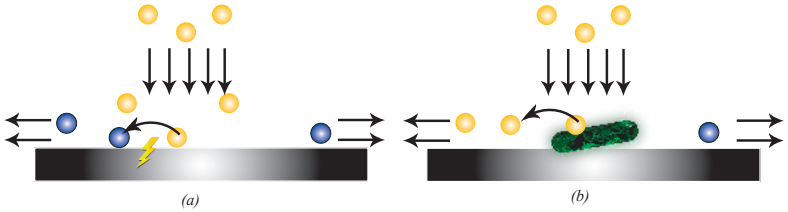

Figure 2-10: Physical blocking of the electrode by bacteria will prevent some but not all of the current transfer. In (a) the default state of the Levich curve measurements all reactants that make it to the surface disk will be oxidized and current will transfer. In (b) the adhered state, any reactants that are blocked by bacteria on the surface and advected away in will not contribute to the current.

2-5, 2-7, 2-8 is likely a physical blocking of the electrode as shown in Figure 2-10. This could be due to bacteria or proteins that block the ferricyanide from reacting at the electrode surface. Assuming that the area a single bacteria occupies is half its surface area, we estimate the number of bacteria adhered as a function of time (Figure 2-11) and the subsequent deposition rate. The number of bacteria adhered to the surface is approximated by taking the initial area ratio,

$$n = \frac{1 - A/A_0}{0.5 \cdot SA_{microbe}}, \tag{2.5}$$

assuming that half of the rod-shaped bacteria is in contact with and blocking the disk and proteins contribute a negligible amount to the blocking. As shown in Table 2.2, the deposition rate of *B. subtilis* oscillates over each cycle unlike *E. coli*, which steadily decreases from the second 30 min cycle, as described in the literature.[32] The values in this work include any proteins secreted into the media or directly onto the substrate, though the deposition rates for *E. coli* K12 are close to those found (50 – 400 $cm^{-2}\,s^{-2}$) for *E. coli* O2K2 on glass at a lower shear rate 0 – 100 s^{-1} in the literature.[48] While we did not find a direct comparison, the adhesion of *B. subtilis* forms biofilms as strongly as *Pseudomonas aeruginosa*, which maintained a near constant 400 $cm^{-2}\,s^{-1}$ over shear rates from 0 - 600 s^{-1}.[48] To compare with traditional methods, we quantify bacteria coverage on the electrode using fluorescence microscopy, following the methods of Shive et al.[11] and Wang et al.[12] for measur-

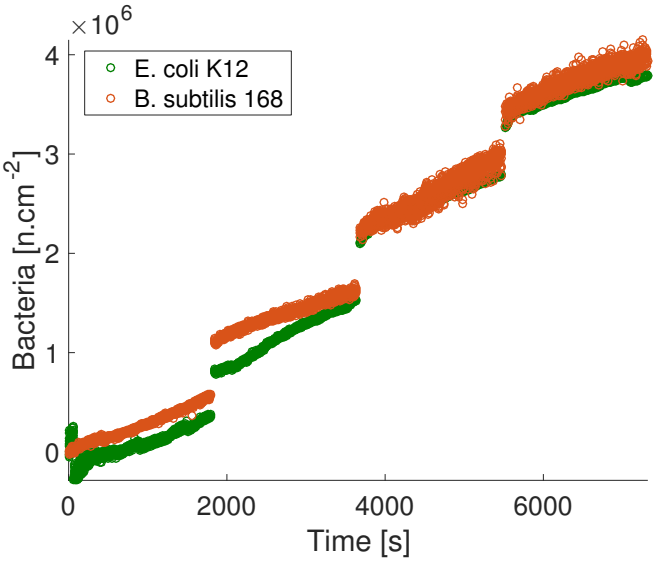

Figure 2-11: Deposition kinetics as a function of time estimated from the rotating disk results (Figure 2-8), for *E. coli* K12 CGSC 4401 and *B. subtilis* 168 BGSC 1A1 on platinum at 30 °C in phosphate-buffered solution amended with 30% glycerol, pH 7.0, at a concentration of $1.97 \pm 0.455 \times 10^8$ cells $\cdot$ cm^{-3} and a wall shear rate of 613 s^{-1}. Linear regression was performed over each interval to estimate deposition rate. All experiments performed in biological triplicate.

Table 2.2: Deposition rates determined from ratio of current

Interval (min)	*E. coli* K12	*B. subtilis* 168
0	242.2 ± 85.0	$297.4 \pm 94.3\,\mathrm{cm}^{-2} \cdot \mathrm{s}^{-1}$
30	439.9 ± 184	287.4 ± 67.0
60	343.5 ± 147	433.3 ± 133.1
90	252.7 ± 75.0	299.9 ± 45.0

Table 2.3: Bacterial surface coverage measured using fluorescence microscopy

Bacteria	Area %(10X)	Area % (20X)	Area % (40X)
E. coli K12	8.1 ± 5.4 %	31 ± 30 %	11 ± 14 %
B. subtilis 168	3.2 ± 2.4 %	6.2 ± 0.8 %	8.3 ± 10 %

ing adhesion (see Figure 2-12a and 2-12b). While common in literature,[32] this visual method is not dynamic and relies on imprecise "slight rinsing" or "dipping" prior to imaging.[32] The results, shown in Table 2.3, are variable with error that is as high or higher than the measured values. Regardless, there is a significant difference between the electrode area that *E. coli* cells cover relative to *B. subtilis* visually. Because *E. coli* covers a significantly larger area, this explains the trend in Figure 2-8 that the two area coverages are close despite *E. coli* being less likely to form a biofilm than *B. subtilis*. The formation of a biofilm is largely a function of exopolymeric substance secretion while the electrochemical methods measure bacterial adhesion in addition to any polymers and proteins secreted by the bacteria which, may inhibit reactant flux to the electrode. The results from this study are likely not translatable to different temperatures, fluids, metals, electrical potentials or bacteria. Instead, the full procedure would be need to be followed to quantify the bacterial deposition rate. As noted in Equation 2.2, the diffusivity and viscosity are temperature dependent. The former should affect adhesion similarly to other methods for determining bacterial adhesion. The advantage here is the independent quantification of how those parameters, and the reaction rate of the tracer chemical, vary and affect the measurement. One of the other promising methods of measuring microbial adhesion is the use of a quartz-crystal microbalance. This technique can measure weight changes down to the 1 ng allowing for the measurement of a single microbe. While very accurate for adhered mass, QCM cannot distinguish area and would measure all three configurations shown in Figure 2-13 as the same. While very accurate for area, the methods described herein could not conclude that that all three configurations contained the same number of bacteria. Though at the shear rates we use, configurations shown in Figure 2-13 (b) and (c) are unlikely.[49] It is possible to incorporate a quartz-crystal microbalance into an RDE which would improve both of the techniques.[50]

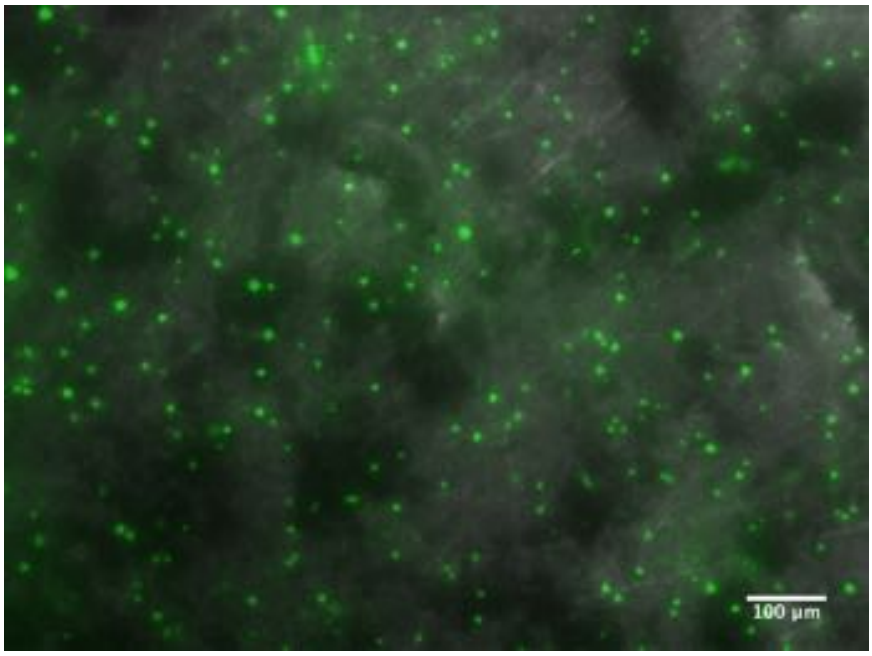

(a) *E. coli* K12

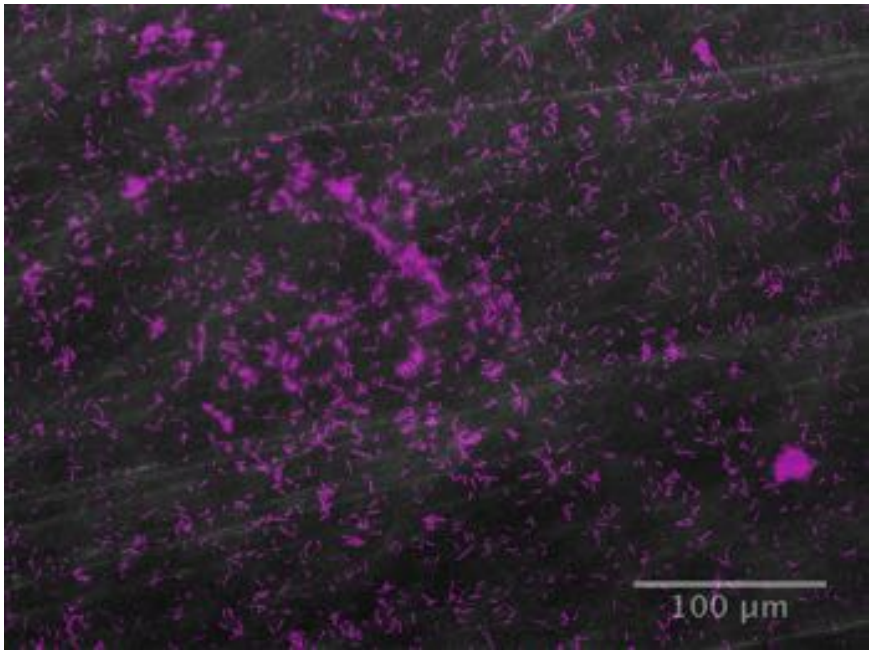

(b) *B. subtilis* 168

Figure 2-12: Fluorescent images over-layed on top of light microscopy of the Pt electrode surface of *E. coli* K12 CGSC 4401 (Figure 2-12a) showing higher surface coverage than *B. subtilis* 168 BGSC 1A1 (Figure 2-12b). Computed values shown in Table 2.3 show some agreement with the data collected by the Levich curve but are explicitly dependent on where the image is taken and implicitly dependent on the rinsing method employed.

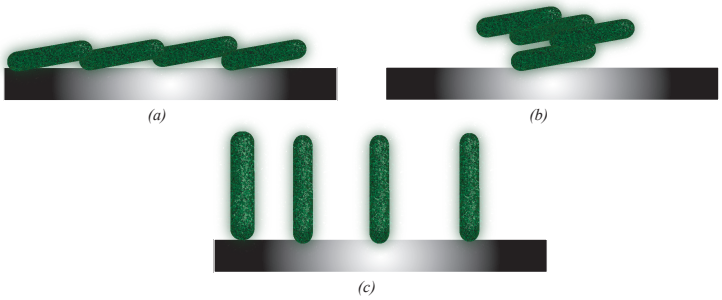

Figure 2-13: Artist representation of QCM and RDE measurement defects. A quartz-crystal microbalance would measure all three microbe configurations as the same, when they are clearly different. The rotating disk measurements described herein would measure all three images as distinct, when each adhesion number is the same. The area covered is an important characteristic for drag reduction and surface coatings, while knowing the number of bacteria is important for determining cytotoxicity. The angle between microbe and surface in configuration (c) is an exaggeration though angles near 60° have been seen.[3]

2.4 Conclusion and Future Work

We use an RDE to extend chronoamperometry's application to detecting microbial adhesion under known mass flux.[51] We show mass transport limiting current and cyclic voltammetry can quantify the onset and quantify the area of bacterial adhesion to metals at known mass flux, over shear rates and time. Unlike microfluidic or microscopic methods, this method can be used with opaque metals and unlike quartz-crystal microbalance this measures occupied area instead of mass.[53, 5, 50] Future work should include incorporation of quartz-crystal microbalance into an RDE to determine how shear, potential and time contribute to microbial orientation on a surface.

We show that deviation from the mass transport limiting current from the Levich curve does not arise from the same physical mechanisms exhibited by mammalian cells or high-density nano-particles. We show that at the concentrations relevant to aquatic environments viscosity does not change, unlike high-density nanoparticles. We show stiffness is likely not a contributing factor to the deviation as both a stiff gram-positive and a less-stiff gram-negative bacterial strain exhibit similar behavior though further study of the effect of particle stiffness could be done using polymers like PDMS. Future

work should also include determining how the soft-layer affects adhesion using mutant strains, fixation, various salinity or protein bound nanoparticles.[52] The deviation of mass-transport limiting current comes from microbial adhesion and the adhesion rates we find are similar to those in the literature for *E. coli* spp. and between two biofilm formers, *P. aeruginosa* and *B. subtilis*. Future study using these methods can be done to address Nealson's [2, 54] hypothesis that surface polarization affects bacterial adhesion since limiting current occurs over a range of potentials determining if shear and surface polarization can prevent biofouling or decrease bioreactor start-up time.[55]

References

[1] Jeffrey S McLean, Greg Wanger, Yuri A Gorby, Martin Wainstein, McQuaid, Jeff, Shun' ichi Ishii, Orianna Bretschger, Haluk Beyenal, and Kenneth H Nealson. Quantification of electron transfer rates to a solid phase electron acceptor through the stages of biofilm formation from single cells to multicellular communities. Environmental Science and Technology, 44(7):2721–2727, 2010.

[2] KH Nealson and SE Finkel. Electron flow and biofilms. Mrs Bulletin, 36(5):380–384, 2011.

[3] Eric Lauga. Bacterial hydrodynamics. Annual Review of Fluid Mechanics, 48(1):105–130, 2016.

[4] A Karimi, D Karig, A Kumar, and AM Ardekani. Interplay of physical mechanisms and biofilm processes: review of microfluidic methods. Lab Chip, 15(1):23–42, 2015.

[5] Hannah H Tuson and Douglas B Weibel. Bacteria–surface interactions. Soft Matter, 9(17):4368, 2013.

[6] MP Schultz, JA Bendick, ER Holm, and WM Hertel. Economic impact of biofouling on a naval surface ship. Biofouling, 27(1):87–98, 2011.

[7] CU Schwermer, G Lavik, RMM Abed, B Dunsmore, TG Ferdelman, P Stoodley, A Gieseke, and D de Beer. Impact of nitrate on the structure and function of bacterial biofilm communities in pipelines used for injection of seawater into oil fields. Applied and Environmental Microbiology, 74(9):2841–2851, 2008.

[8] M Sadekuzzaman, S Yang, MFR Mizan, and SD Ha. Current and recent advanced strategies for combating biofilms. Comprehensive Reviews in Food Science and Food Safety, 14(4):491–509, 2015.

[9] JW Daily and RE Nece. Chamber dimension effects on induced flow and frictional

resistance of enclosed rotating disks. Journal of Basic Engineering, 82(1):217, 1960.

[10] P Bernabeu, Luc Tamisier, De A Cesare, and Adrien Caprani. Study of the adsorption of albumin on a platinum rotating disk electrode using impedance measurements. Electrochimica Acta, 33(8):1129–1136, 1988.

[11] Matthew S Shive, Sakeena M Hasan, and James M Anderson. Shear stress effects on bacterial adhesion, leukocyte adhesion, and leukocyte oxidative capacity on a polyetherurethane. Journal of Biomedical Materials Research, 46(4):511–519, 1999.

[12] I w Wang, JM Anderson, and RE Marchant. Staphylococcus epidermidis adhesion to hydrophobic biomedical polymer is mediated by platelets. Journal of Infectious Diseases, 167(2):329–336, 1993.

[13] Allen J Bard and Larry R Faulkner. Electrochemical Methods. John Wiley & Sons Incorporated, 2nd edition, 2001.

[14] Philippe Mandin, Th Pauporté, Ph Fanouillère, and D Lincot. Modelling and numerical simulation of hydrodynamical processes in a confined rotating electrode configuration. Journal of Electroanalytical Chemistry, 565(2):159–173, 2004.

[15] L'Hostis, E, C Compére, D Festy, B Tribollet, and C Deslouis. Characterization of biofilms formed on gold in natural seawater by oxygen diffusion analysis. Corrosion Science, 53(1):1–7, 1997.

[16] DJ Schiffrin and De SR Sanchez. The effect of pollutants and bacterial microfouling on the corrosion of copper base alloys in seawater. Corrosion, 41(1):31–38, 1985.

[17] Jerome T Babauta and Haluk Beyenal. Mass transfer studies of geobacter sulfurreducensbiofilms on rotating disk electrodes. Biotechnology and Bioengineering, 111(2):285–294, 2013.

[18] Sebastian P Bonanni, Dan F Bradley, Germán D Schrott, and Juan Busalmen. Limitations for current production in geobacter sulfurreducens biofilms. ChemSusChem, 6(4):711–720, 2013.

[19] de Ficquelmont-Loizos, May, Luc Tamisier, and Adrien Caprani. Mass transfer in laminar flow at a rotating disk electrode in suspensions of inert particles. Journal of The Electrochemical Society, 135(3):626, 1988.

[20] Osman Sara, F İçer, Sinan Yapici, and Bayram Sahin. Effect of suspended CuO nanoparticles on mass transfer to a rotating disc electrode. Experimental Thermal and Fluid Science, 35(3):558–564, 2011.

[21] Adrien Caprani, May de Loizos, Luc Tamisier, and Pierre Peronneau. Mass transfer in laminar flow at a rotating disk electrode in suspensions of inert particles II . theoretical evaluation of experimental results. Journal of The Electrochemical Society, 135(3):635–642, 1988.

[22] Benjamin G Levich. The theory of concentration polarisation. Discussions of the Faraday Society, 1:37–49, 1947.

[23] Jerome T Babauta, Hung Nguyen, Timothy Harrington, Ryan Renslow, and Haluk Beyenal. pH, redox potential and local biofilm potential microenvironments within geobacter sulfurreducens biofilms and their roles in electron transfer. Biotechnology and Bioengineering, 109(10):2651–2662, 2012.

[24] Haydée Becerra, C Retamoso, and Digby D Macdonald. The corrosion of carbon steel in oil-in-water emulsions under controlled hydrodynamic conditions. Corrosion Science, 42(3):561–575, 2000.

[25] Jung Kim, Booki Min, and Bruce E Logan. Evaluation of procedures to acclimate a microbial fuel cell for electricity production. Applied microbiology and biotechnology, 68(1):23–30, 2005.

[26] William M Haynes. CRC handbook of chemistry and physics. CRC Press, 2014.

[27] R Woods. Hydrogen adsorption on platinum, iridium and rhodium electrodes at reduced temperatures and the determination of real surface area. Journal of Electroanalytical Chemistry and Interfacial Electrochemistry, 49(2):217–226, 1974.

[28] Xuanhao Sun, William D Weinlandt, Harsh Patel, Mingming Wu, and Christopher J Hernandez. A microfluidic platform for profiling biomechanical properties of bacteria. Lab on a Chip, 14(14):2491–2498, 2014.

[29] Frederick M Ausubel, Roger Brent, Robert E Kingston, David D Moore, JG Seidman, John A Smith, and Kevin Struhl, editors. Current Protocols in Molecular Biology. John Wiley & Sons, Inc, 2003.

[30] Burt Bronk, Willem Merwe, and Marc Stanley. In vivo measure of average bacterial cell size from a polarized light scattering function. Cytometry, 13(2):155–162, 1992.

[31] Ian B Butler, Martin A. A. Schoonen, and David T Rickard. Removal of dissolved oxygen from water: a comparison of four common techniques. Talanta, 41(2):211–215, 1994.

[32] Henk J Busscher and Henny C van der Mei. Microbial adhesion in flow displacement systems. Clin Microbiol Rev, 19(1):127–141, 2006.

[33] Bernard Tribollet, John Newman, and William H Smyrl. Determination of the diffusion coefficient from impedance data in the low frequency range. Journal of The Electrochemical Society, 135(1):134, 1988.

[34] Bruin Roffel and Jan J van de Graaf. The diffusion coefficient of ferricyanide ions in aqueous potassium chloride solutions with and without polyethylene oxide addition. J Chem Eng Data, 22(3):300–302, 1977.

[35] SJ Konopka and McDuffie, Bruce. Diffusion coefficients of ferri- and ferrocyanide ions in aqueous media, using Twin-Electrode Thin-Layer electrochmistry. Analytical Chemistry, 42(14):1741–1746, 1970.

[36] GK Batchelor. The effect of brownian motion on the bulk stress in a suspension of spherical particles. Journal of Fluid Mechanics, 83(01):97–117, 1977.

[37] J Buongiorno. Convective transport in nanofluids. Journal of Heat Transfer, 128(3):240–250, 2006.

[38] Adrien Caprani, May de Loizos, and M Nakache. On the effects of particles in suspension on the mass transfer exchange area at a rotating disc electrode. PhysicoChemical Hydrodynamics, 6:567–578, 1985.

[39] JM Meinders, Van HC der Mei, and HJ Busscher. Deposition efficiency and reversibility of bacterial adhesion under flow. Journal of Colloid and Interface Sciences, 176:329–341, 1995.

[40] H Ozbek, JA Fair, and SL Phillips. Viscosity of aqueous sodium chloride solutions from 0-150°C, 1977.

[41] Brian M Haines, Andrey Sokolov, Igor S Aranson, Leonid Berlyand, and Dmitry A Karpeev. Three-dimensional model for the effective viscosity of bacterial suspensions. Physical Review E, 80(4):041922–7, 2009.

[42] PJ Sonneveld, W Visscher, and E Barendrecht. The influence of suspended particles on the mass transfer at a rotating disc electrode. non-conducting particles. Journal of Applied Electrochemistry, 20(4):563–574, 1990.

[43] H Brenner. The stokes resistance of a slightly deformed sphere. Chemical Engineering Science, 19(8):519–539, 1964.

[44] Thaddeus J Coin and John S Olson. The rate of oxygen uptake by human red blood cells. The Journal of biological chemistry, 254(4):1178–1190, 1979.

[45] Peter Ertl, Birgit Unterladstaetter, Karl Bayer, and Susan R Mikkelsen. Ferricyanide reduction by escherichia coli: kinetics, mechanism, and application to the optimization of recombinant fermentations. Anal Chem, 72(20):4949–4956, 2000.

[46] Arnold Bisschop, Johannes Boonstra, Herman J Sips, and Wil N Konings. Respiratory chain linked ferricyanide reduction drives active transport in membrane vesicles from bacillus subtilis. FEBS Letters, 60(1):11–15, 1975.

[47] Shawn D Ryan, Brian M Haines, Leonid Berlyand, Falko Ziebert, and Igor S Aranson. Viscosity of bacterial suspensions: Hydrodynamic interactions and self-induced noise. Physical Review E, 83(5):050904–4, 2011.

[48] Astrid Roosjen, Niels P Boks, Henny C van der Mei, Henk J Busscher, and Willem Norde. Influence of shear on microbial adhesion to PEO-brushes and glass by convective-diffusion and sedimentation in a parallel plate flow chamber. Colloids and Surfaces B: Biointerfaces, 46(1):1–6, 2005.

[49] L Stappers, MG Basavaraj, J Vermant, and J Fransaer. Flow alignment of prolate particles on a rotating disk electrode. Journal of The Electrochemical Society, 153(9):C660, 2006.

[50] Ying Liu, Antonio Berná, Victor Climent, and Juan Feliu. Real-time monitoring of electrochemically active biofilm developing behavior on bioanode by using EQCM and ATR/FTIR. Sensors and Actuators B: Chemical, 209:781–789, 2015.

[51] Boulangé-Petermann, Laurence, Bellon-Fontaine, Marie-Nöelle, and Bernard Baroux. An electrochemical method for assessing biodeposition on stainless steel. Journal of Microbiological Methods, 21(1):83–96, 1995.

[52] Naga Dingari and Cullen R Buie. Theoretical investigation of bacteria polarizability under direct current electric fields. Langmuir, 30(15):4375–4384, 2014.

[53] Margot Vigeant, Roseanne M Ford, Michael Wagner, and Lukas K Tamm. Reversible and irreversible adhesion of motile escherichia coli cells analyzed by total internal reflection aqueous fluorescence microscopy. Appl Environ Microb, 68(6):2794–2801, 2002.

[54] Kenneth H Nealson and Annette R Rowe. Electromicrobiology: realities, grand challenges, goals and predictions. Microbial Biotechnology, 9(5):595–600, 2016.

[55] Xin Wang, Yujie Feng, Nanqi Ren, Heming Wang, He Lee, Nan Li, and Qingliang Zhao. Accelerated start-up of two-chambered microbial fuel cells: effect of anodic positive poised potential. Electrochimica Acta, 54(3):1109–1114, 2009.

Chapter 3

Separating the influence of shear from mass transport on exoelectrogenic biofilms

3.1 Introduction

Microbes variously termed exoelectrogens,[1] electricigens,[2] or electroactive [3] can use insoluble mediators as terminal electron acceptors. These include *Geobacter sulfurreducens*,[4] and *Shewanella onedensis*, [5] utilizing insoluble metals like magnesium oxide and iron oxide. These microbes can grow to greater thickness [6] and stay more active [7, 8] than soluble respiring microbes because their electron acceptor is always accessible. In an engineered environment, like bioelectrochemical cells, corrosion resistant metals, like carbon [9], stainless steel [10], and titanium [11] are used, to collect the electrons and pass them through a circuit to do work. While beneficial to engineers, this creates pH stress differing from the naturally occurring charge neutral process where the reduced metal combines with the released protons.[6] To solve this challenge, some bioelectrochemical systems use forced convection as the predominate means of mass transport [12, 13, 14, 15] and many lab scale bioelectrochemical systems use stir bars even when not explicitly stated. Bonanni et al., [16] showed that

convection of substrate through the biofilm is negligible as should be expected with biofilm pore size [17, 18, 19]. Yet, they did not distinguish the competing factors of shear stress from mass transport. Rotating disc systems can be used to simulate many practical flow systems, like pipe, channel, and porous media flow, while decoupling mass transfer from shear.[20]

We use rotating disk electrodes to study the metabolic and structural response of electroactive microbial biofilms to shear stress. A rotating disk electrode (RDE) consists of a multi-flanged glass flask and a disk mounted in a shaft rotating under precision motor control. The solutions to equations of fluid flow and mass transfer at a rotating disk are analytical asymptotic expansions that allow for fast, agile, and accurate comparisons between theory and experiment. [21, 22] This also allows predictable control of the fluid shear rate interacting with a biofilm grown on the disk independent from the mass flux. As the shear rate changes a biofilms' respiration changes [23]. An electroactive biofilm should manifest this change as a change in current as an *in situ* measurement of its metabolism.[24, 25] Similarly biofilms change the amount of biomass produced under shear; we expect the porosity of an electroactive biofilm will similarly change with corresponding evidence in their electrochemical impedance.[26] We grow *Geobacter sulfurreducens*, an obligate anaerobe that directly respires on metals, for 7 days on the RDE at a fixed rate of rotation in fed-batch mode under positive $N_2|CO_2$ pressure. At the end of the measurement, we fix and stain the biofilm in preparation for imaging. We use confocal microscopy to measure the porosity of the biofilm as a function of depth. These images are analyzed using MATLAB and the relative biofilm density as a function of depth is compared to an empirical model based on a finite set of dimensionless variables. Using the current output and resistance measurements from the rotating disk electrode and coupling that with the pore structure, we test whether the biofilm has adopted an optimal structure for metabolism or if the biofilm structure serves other, yet to be determined purposes.

3.2 Methods

3.2.1 Practical Benchmark

We benchmark this study to the up-flow microbial fuel cell by He et al.[12] An up-flow microbial fuel cell is designed in a similar manner to an up-flow anaerobic sludge blanket bioreactor where organic laden fluid is flown upwards over a biofilm-coated porous media, having a smaller footprint than continuous stirred tank reactors and subsequently higher shear.[27] Matching two systems using only the Reynolds number produces vastly different results between the two systems.[28, 20]. Instead, both the mass flux and the momentum flux must be matched. To do this, we compare the rotating disc electrode system to membrane bioreactors and packed bed reactors using theories of flow through porous media. The superficial velocity, U_0 is defined as

$$U_0 = \frac{Q}{A_r} \tag{3.1}$$

where Q is the total flow rate and A_r is the area of the empty reactor. The Reynolds number for the flow is defined as

$$Re_p = \frac{U_0}{(1-\phi)S_V\nu}, \tag{3.2}$$

where the specific surface area to volume ratio, S_V and porosity ϕ must be measured.[29] The shear stress, τ, on particles in the porous media is then calculated as [29]

$$\tau_p = \frac{1}{S_v}\frac{\phi}{(1-\phi)}\frac{\mu}{k_p}U_0. \tag{3.3}$$

The permeability, k_p, is typically measured, yet can be calculated using the Kozney-Carman equation as [30],

$$k_p = \frac{\phi^3}{K(1-\phi)^2 S_V^2} \tag{3.4}$$

Table 3.1: Properties of porous media, reticulated vitreous carbon foam, and flow parameters used in an anode of an Up-flow Microbial Fuel Cell from He et al., [12].

ϕ	$A[\mathrm{cm}^2]$	$S_V[\mathrm{m}^{-1}]$	$k[\mathrm{m}^2]$	$Q[\mathrm{m}^3 \cdot \mathrm{s}^{-1}]$	$U_0[\mathrm{m} \cdot \mathrm{s}^{-1}]$
0.97	26	51.05	0.0779	7.56×10^{-7}	2.9×10^{-4}

where $K \approx 5$ is the value typically used for the Kozney constant [30]. The dimensionless stress similarly found with the fluid inertia is then [29]

$$\frac{\tau_p}{\frac{1}{2}\rho U_0^2} = \frac{2K}{\phi^2} Re_p^{-1}. \tag{3.5}$$

The similarity to pipe flow scaled by the porosity and Kozney constant is expected since flow through porous media has been related to flow through packed tubes.[31, 29]

Using values from literature, Table 3.1, it is possible to determine a dimensionless shear stress that is common between the two systems. The dimensionless shear stress is then $\tilde{\tau}_p = 0.056$. This value can be matched to the shear from Equation A.8 to rotating disc setups and for our system results in a rotation rate of 739 rpm, a shear stress of 1.048 Pa and shear rate of 1046 s^{-1}.

Mass transport equation for pipe flow

$$N_p = 0.844 c_\infty D_0 Re_p^{1/3} Sc^{1/3} \left(\frac{D_p^{-2}}{L}\right)^{1/3}, \tag{3.6}$$

where we have used the porous Reynolds number, Re_p, and the porous diameter is D_p,

$$D_p = \frac{\phi}{(1-\phi)S_v}. \tag{3.7}$$

Using the data from He et al.,[12] the flux can be found $N_p = 5.35 \times 10^{-6}\,\mathrm{gCOD} \cdot \mathrm{cm}^{-2} \cdot \mathrm{s}^{-1}$. We can use Equation A.16 to fix the mass flux for the various shear stress conditions, summarized in Table 3.2 In 2, we described how mass transport limiting current is affected by the adhesion of bacteria to the electrode. We use the initiation rotation rate we found, 600 RPM, to normalize any indiscriminate adhesion before establishing the shear condition.

Table 3.2: The experimental parameters used for an acetate-fed *Geobacter* rotating disk. The top row is based on the experimental parameters of He et al., scaled as described herein.[12]

Rotation Rate	Shear	COD	Concentration	Dimensionless Shear
[rpm]	$[\text{dynes} \cdot \text{cm}^{-2}]$	$[\text{gCOD} \cdot \text{L}^{-1}]$	[mM]	[]
739	10.46	0.96	14.97	0.0562
159	1.046	2.06	32.24	0.1211
34	0.1046	4.45	69.47	0.2610

The current, i, will be normalized to the mass transfer limiting current for a rotating disk, i_{lim} from Equation A.19,

$$\frac{i}{i_{lim}} = \frac{i}{n_e F A N} = i \left(n_e F A L_c \nu^{-1/6} \omega^{1/2} c_\infty D_0^{2/3} \right)^{-1}, \tag{3.8}$$

To correlate this with the flux through the biofilm, the growth time of the biofilm is taken into account as

$$t Y q_m, \tag{3.9}$$

where Y is the biomass yield of the substrate and q_m is the maximum substate utilization rate [32]. A plot of i/i_{lim} versus tYq_m at constant mass flux results in curve that is similar to that of logistic growth with parameters that may relate to physical mechanisms that should be explored. Looking for mechanical explanations biological phenomena may not be as farfetched as one would assume at first glance. Nadell et al., were able to explain many examples of biofilm cooperation as manifestations of competition, mutualism, or resulting from environmental conditions [33].

3.2.2 Media

The media was 0.59 g KH_2PO_4, 0.38 g KCl 2.19 g $NaHCO_3$, 0.36 g NaCl, 0.20 g NH_4Cl, 0.04 g $CaCl_2 \cdot 2\,H_2O$, and 0.10 $MgCl_2 \cdot 6\,H_2O$ (MilliporeSigma, Darmstadt, GER) in 1 L of deionized water based on the media used in bioelectrochemistry experiments.[34, 35] The resulting conductivity was $2.10\,\text{mS}\,\text{cm}^{-1}$ at 30 °C. To this

media was added 14.97 mL, 32.24 mL, or 69.47 mL of 1 M sodium acetate in the same media. This resulted in a slight increase in conductivity from 5.5 to 6.7 $\mathrm{mS\,cm^{-1}}$ from lowest to .

3.2.3 Electrodes

A 0.4 cm diameter graphite exchange disk working electrode (Pine Instruments, Durham, NC, USA) was used as the working electrode. The electrode was soaked in 1 M hydrochloric acid and 1 M sodium hydroxide at for 24 hours after wiping with ethanol and roughened using 5 μm grit silicon carbide polishing paper to clean from from previous experiments. A single junction Ag/AgCl (3.8 M KCl) reference electrode (MilliporeSigma, Darmstadt, GER) was used because the conductivity of the media is too low to sustain a double-junction. While this may cause leakage of the 3.8 M sodium solution into the electrolyte, the abiotic experiments do not show any significant deviation. A 0.1 cm diameter graphite electrode behind a glass frit was used as the counter electrode (Pine Instruments, Durham, NC, USA).

3.2.4 Apparatus

The reactor was a water jacketed inverted 500 mL Erlenmeyer flask, with 4 ports for electrodes and gas (Pine Instruments, Durham, NC, USA), see Figure 1. The reactor was maintained at a constant temperature of 30 °C using a water jacket (Julabo E5, Julabo USA, Allentown, PA, USA). The system was purged and blanketed at 50 sccm with ultra-high purity 80% nitrogen and 20% carbon dioxide gas (Airgas Inc, Radnor Twp, PA, USA). The current was measured with a Gamry Reference 600 or a Gamry Reference 3000 (Gamry Instruments, Philadelphia, PA, USA) with a resolution of 600 mA and a bandwidth of 10 MHz which is much lower than the sampling rate and current measured.

3.2.5 Bacteria

Geobacter sulfurreducens strain PCA (ATCC) was grown anaerobically from a frozen stock in a media matching Coppi et al., with 4 mM L-cystine and 40 mM fumarate [34] at 30 °C. This was transferred to a 100 mL flasks and grown for 2 days, the cells were centrifuged twice at 6000 rpm for 10 min rinsed in between with the media described earlier.

3.2.6 Procedure

The media was brought to temperature 30 °C and internal resistance of the media was measured. All conditions were run in biological triplicate. A roughly 24 hr cycle included 30 min open circuit potential measurement, followed by two cycles of cyclic voltammetry, chronoamperometry for 22 hours, and electrochemical impedance spectroscopy. Chronoamperometry was conducted at $-0.156\,\mathrm{V}$ vs Ag/AgCl based on Soussan et al.[36] Open circuit potential was measured at a sampling rate of 0.016 Hz for 30 min as this appeared sufficient to reach steady state. similar to Bernabeu et al., for serum binding versus shear on a plexiglass coated platinum cylinder that showed that initial adsorption occurred within 3-5 minutes [37]. Cyclic voltammetry had an equilibration time of 5 s, a step size of 2 mV and a scan rate of $1\,\mathrm{mV\,s^{-1}}$ from $-0.755\,\mathrm{V} - -0.045\,\mathrm{V}$ vs Ag/AgCl. following the method of Marsili et al.[38]

We measure the electrical impedance of the biofilm since it may be related to the structure of the biofilm.[16, 39] The impedance is a key characteristic of microbial fuel cells that can be used to diagnose their performance.[40] Electrochemical impedance spectroscopy was conducted using two sets of parameters 1000000 Hz to 0.10 Hz at $E_{dc} = -0.340\,\mathrm{V}$ vs Ag/AgCl, $E_{ac} = 5\,\mathrm{mV}$ and 1000000 Hz to 0.01 Hz at $E_{dc} = -0.157\,\mathrm{V}$ vs Ag/AgCl, $E_{ac} = 10\,\mathrm{mV}$ following both Babauta and Beyanal and Marsili et al.[35, 38]

The biofilm density and thickness are necessary to compare the results to previous research on bioreactors.[41] After 7 days, the bacteria on disk were dyed using 4',6-diamidino-2-phenylindole a DNA stain and Alexa Fluor®594 -Concanavalin A,

Conjugate that binds to glycocalyx.[18] After 10 minutes, the cells were fixed for 24 hrs using 4 % glutaraldehyde solution in their native buffer. The biofilm was then rinsed in an ethanol series 30, 50, 70, 90, 100, 100. These were imaged using confocal microscopy on using a 10X objective across the entire disk and then using a 40X objective at the center. The sample was then critical point dried and sputter coated for imaging using SEM. The images were processed in MATLAB to find porosity was calculated layer by layer and overall surface roughness. Using AFM to measure roughness resulted in too much noise because the EPS matrix collapses after drying resulting in many more holes.

3.3 Results and Discussion

We continuously measure the effects of shear at fixed mass flux on electroactive biofilms. Bacteria start to adhere within the first 30 minutes under shear ([42], and Chapter 2). This is followed by faster rates of adhesion as more adhesion sites are opened up by proteins from failed adhesion events, protein secretion, and recruitment molecules. [42] While little of this information is captured by our current experimental procedure, initial adhesion of viable bacteria can be seen in the sharp decrease of the initial chronopotetiometry at open circuit, Figure 3-1 relative to the abiotic controls. This is expected with *Geobacter sulfurreducens* on graphite and while they all eventually reach the same point, future work should determine how persistent the difference in the rate of initial polarization is for each rotation rate and how this is proportional to the number of adhered organisms. [43] As the growth rate of *Geobacter sulfurreducens* strain PCA is $Yq_m = 9.2 \times 10^{-6}\,\mathrm{s}^{-1}$ most of the bacteria found on the electrode at this point likely came from the solution [32]. For the same reason, current over the first 24 hrs is also evidence of bacterial adhesion, see Figure 3-2. This near immediate response in current is also found by others,[44] though we find that at higher shear rates, the rate of current increase is higher. We did not fix bacterial concentration, instead relying on growth stage 48 hrs after a 10:1 dilution in 40 mM fumarate. This lack of fixed initial concentration may account for some of the devi-

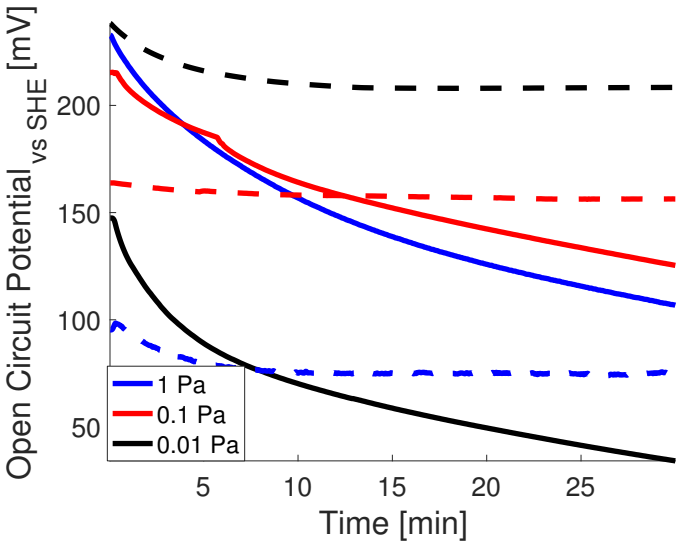

Figure 3-1: Average initial open circuit potential shows adhering metabolically active bacteria. Dashed '–' lines are the abiotic control at the same rotation rates and concentrations as the solid line experiments.

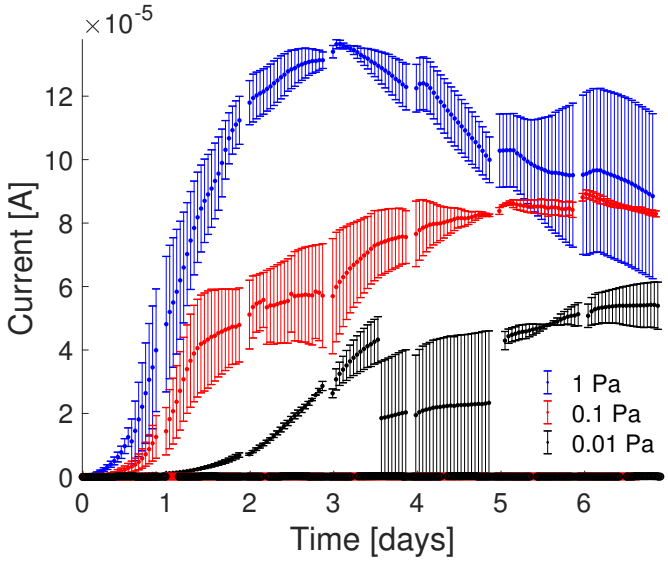

Figure 3-2: The current, at three shear stress conditions 1 Pa, 0.1 Pa and 0.01 Pa. The flux was fixed to an up-flow microbial fuel cell (He et al., [12]) which also corresponded to the 1 Pa shear stress. We can conclude the previous study was likely being run under optimal conditions for maximal current generation. Yet, we find that at the lower shear stress the maximum current persists longer. We found, but did not test further, that the maximal current at the highest shear stress could be maintained if the flux away from the biofilm is increased while the flux towards the biofilm is held constant. The test apparatus is not designed for these conditions. The maximum current we found was $136.55 \pm 2.15\mu$A, $90.234 \pm 1.89\mu$A and $48.578 \pm \mu$A for 1 Pa, 0.1 Pa, and 0.01 Pa respectively.

ation, though not as much as we see here.[44] A biofilm that took 7 days to achieve the same amount of current as reported here at 24 hr ($\sim 2\,\mathrm{A}$) at 1 Pa was imaged, Figure 3-3a. While poorly performing, the biofilm showed growth that agrees well with the streamlines predicted by von Kármán for flow at a rotating disk showing strong fluid influence. Further work should be done to measure the geometric and transcriptomic changes that may be occurring over time in addition to the electrical which is measured in this work.

The current at three shear stresses tested of 1 Pa, 0.1 Pa and 0.01 Pa are shown in Figure 3-2. We can conclude He et al.,[12] was likely being run under optimal conditions for maximal current generation. Yet, we find that at the lower shear stress the maximum current persists longer. If we assume that current is proxy for metabolic rate [25], our results agree with those found for other biofilms that higher shear induces higher metabolic rates.[45] Trulear and Characklis [45] did not test beyond 60 hrs so it is unknown whether similar trade offs between stability and maximum occurred. We found, but did not test further, that the maximal current at the highest shear stress could be maintained if the flux away from the biofilm is increased while the flux towards the biofilm is held constant. The test apparatus is not ideally designed for these conditions. The maximum current we found was $136.55 \pm 2.15\mu$A, $90.234 \pm 1.89\mu$A and $48.578\pm\mu$A. Comparison with Babauta and Beyenal 29 who operated with a similar reactor design, same diameter electrode shows the importance of matching flux conditions in shear dependent studies. While their maximal current at 0.01 Pa and lower flux is higher than ours, at 0.1 Pa and lower flux it is the same, and at 0.63 Pa and lower flux it is lower than our 1.0 Pa and appears to be leveling off. This could also be due to our operation at 43 mV vs SHE based on Soussan et al., [36] while they operated at 500 mV vs SHE. Soussan et al., achieved a much higher current density $1.9\,\mathrm{mA\,cm^{-2}}$ compared with our $1.0\,\mathrm{mA\,cm^{-2}}$ which may be due to the electrochemical adaption of their tested *Geobacter* spp. The open circuit potential is a function of the oxidation state of the biofilm.[47] To the authors knowledge it is not known how many microbes must be metabolically active on the electrode to reach the steady-state redox potential, though it appears to be a function

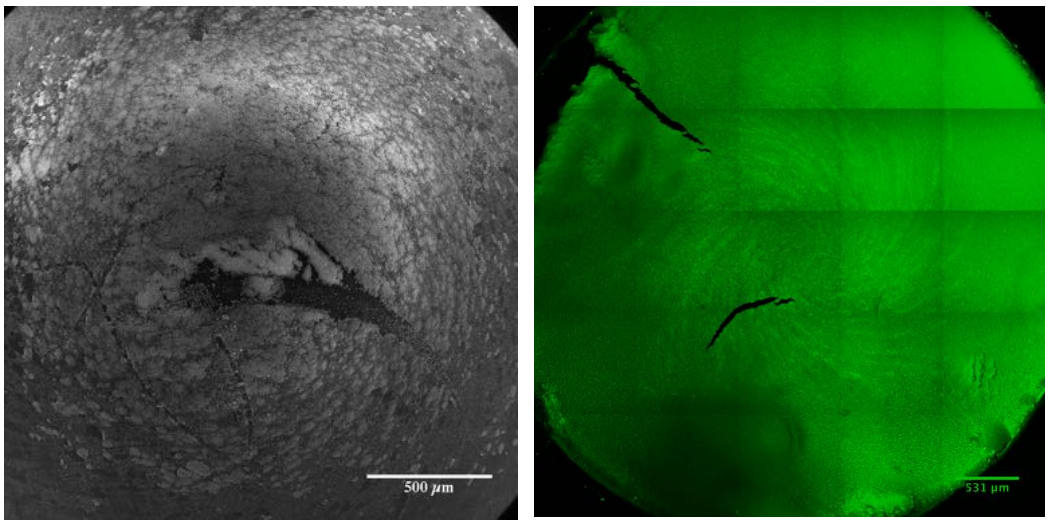

(a) SEM image of Biofilm (b) Confocal image of Biofilm

Figure 3-3: Figure 3-3a is an SEM of a biofilm from an underperforming 1 Pa shear stress experiment: $0.12\text{mA} \cdot \text{cm}^{-2}$, $16\,\mu\text{A}$ after 7 days versus the $1.0\,\text{mA}\,\text{cm}^{-2}$ shown in Figure 3-2. The biofilm shows a growth pattern very similar to the streamlines predicted by the von Kármán solution to flow at a rotating disk. Subsequent biofilms do not reveal any of these patterns with the imaging techniques employed. Figure 3-3b is a slice 6 μm from the surface of an electroactive biofilm taken after 7 days at 0.1 Pa shear stress. This shows the same streamline pattern as seen in Figure 3-3a though the image becomes uniform at further distances. Internal structural memory of biofilms has been seen [46], though this is the first example under controlled conditions to the author's knowledge.

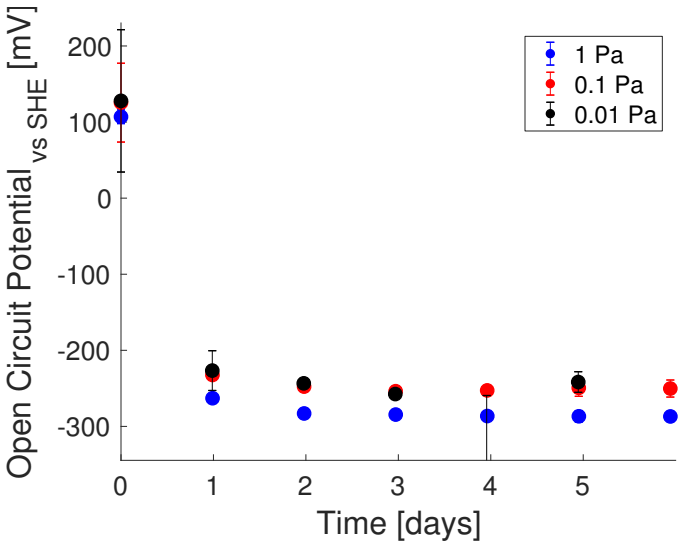

Figure 3-4: The open circuit voltage falls to -266 ± 25 mV vs SHE after one day and is stable throughout the course of the experiment. This value agrees with that found by Bond and Lovley, [49] -420 mV vs Ag/AgCl assuming saturated KCl as the filling electrolyte and subsequent studies on *G. sulfurreducens* strain PCA. This is expected, indicating that the bacteria have colonized and are respiring on the electrode.

of activity and quantity.[48] This potential is fixed by the redox potential terminal electron reaction of the pili/cytochromes that are attached to the electrode. We see (Figure 3-4) that after 24 hrs, the open circuit potential is stable at -266 ± 25 mV vs SHE. This value agrees with that found by others [49, 47] for *G. sulfurreducens* consuming acetate, -420 mV vs Ag/AgCl,[49] assuming their reference electrode was filled with saturated KCl.

A mature electroactive biofilm can be characterized using cyclic voltammetry which shows how rapidly the electron donor can be turned over [50, 51]. For electrochemical reactants suspended in solution, rotation is typically turned off during the scan [52] because reactants and products would be swept away. For an electroactive biofilm, the redox chemicals are adhered to the electrode and at higher scan rates, the different redox proteins can be investigated. We use a single scan rate and find -160 ± 5 mV vs SHE in our work, Figure 3-5, compared with -145 ± 10 mV vs SHE by Richter et al., (2009). [51] It is stable within a standard deviation for each condition past day 3. The values were calculated from cyclic voltammograms taken

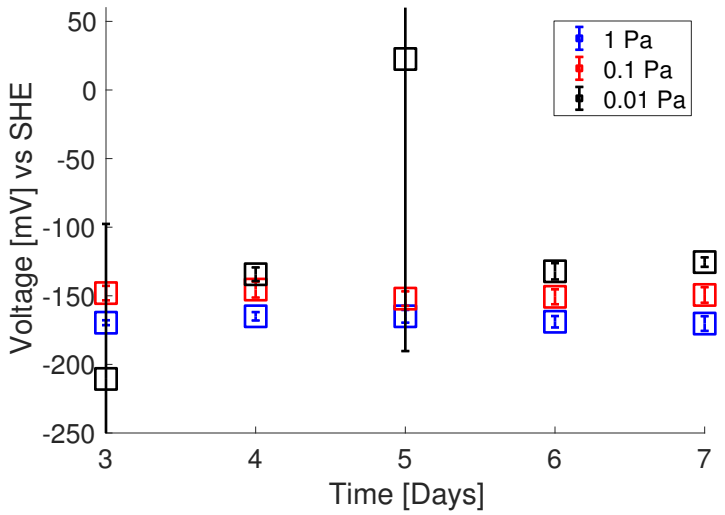

Figure 3-5: Terminal donor formal potential over time across shear. The formal potential of the terminal cytochrome is 160 ± 5 mV vs SHE in our work vs 145 ± 10 mV vs SHE by Richter et al., (2009).[51] It is stable within a standard deviation for each condition past day 3. The values were calculated from cyclic voltammograms taken once a day after a 30 min open circuit potential measurement at $2\,\mathrm{mV} \cdot \mathrm{s}^{-1}$ from the second of 2 cycles.

once a day after a 30 min open circuit potential measurement at $2\,\mathrm{mV} \cdot \mathrm{s}^{-1}$ from the second of 2 cycles.

The electron diffusion current, Figure 3-6, is measured as the maximal current generated during a slow cyclic voltammetry scan. Richter et al., (2009) [51] found a maximum electron diffusion current of 0.17 ± 0.005mA. The expression they found for the electron diffusion current was

$$i_d = nFAk[\mathrm{Mic}][\mathrm{Med}] \tag{3.10}$$

where i_d is the diffusion current, k is the electron transfer rate, [Mic] is the microbe concentration and [Med] is the mediator concentration. We are not able to quantify the amount of redox mediators present nor their reaction rate so we are not able to quantitatively assess the nature of the diffusion current using the expression given. We note that the same trend in the diffusion current agrees with the trend in overall current, Figure 3-2 and in the EIS, Figure 3-8.

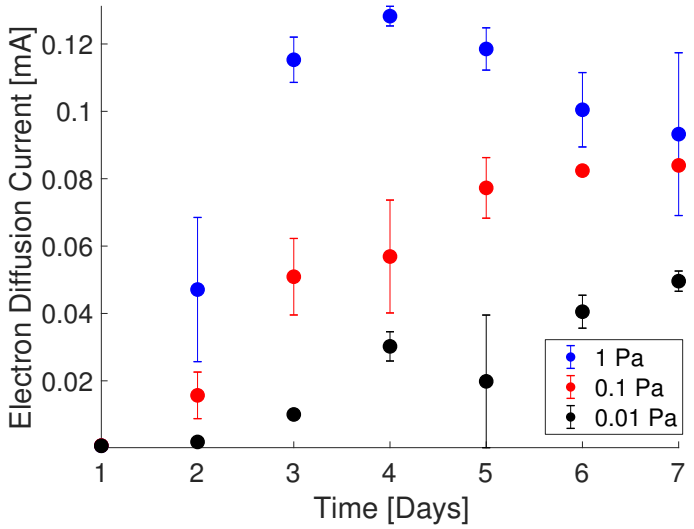

Figure 3-6: Electron diffusion current overtime and across shear. The electron diffusion current is measured as the maximal current generated during a slow cyclic voltammetry scan. Richter et al., (2009) [51] found a maximum electron diffusion current of 0.17 ± 0.005mA. We are not able to quantify the amount of redox mediators present nor their reaction rate so we are not able to quantitatively assess the nature of the diffusion current using the expression given. Though we are able to note that the same trend in overall current matched the diffusion current.

The last measurement made is the electrochemical impedance spectroscopy. This measurement quantifies the complex impedance to charge transfer of the biofilm.[53] There are subtle differences between each abiotic cells because of differences in conductivity of the background media as described in the Methods, Figure 3-7. This linear relationship between the imaginary and real parts of the impedance indicate that there is only mass transfer resistance as should be expected because there are no other charge carriers and acetate is poorly oxidized on a graphite electrode.

The decrease in electron transfer impedance follows the electron diffusion current closely as expected. There is an increase in impedance from day 3 to day 7 of the 1 Pa case but not the other two shear stress conditions. The absence of the increase in the 0.1 Pa and 0.01 Pa conditions clarifies that the steady state seen in both electron diffusion and chronoamperometry has not started to decrease. The increase in impedance may be due to decrease in redox proteins from loss of or death of cells, decrease in the biofilm pH which may cause a loss of conductivity and/or metabolic

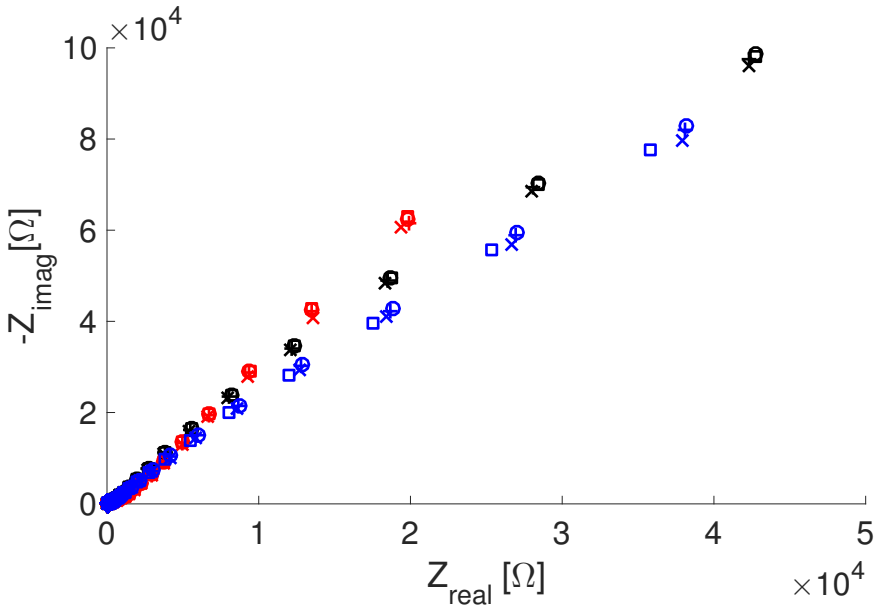

Figure 3-7: The electrochemical impedance spectrum of the system under abiotic conditions. The system only exhibits resistance as there are no reactions occurring at the disk. The differences at low frequencies are due to the differences in conductivity referred to in Methods section as we did not adjust for the increase in from increasing acetate concentration. The color scheme is the same as previous figures, 1.0 Pa - blue, 0.1 Pa - red, 0.01 Pa - black while each symbol corresponds to a different day.

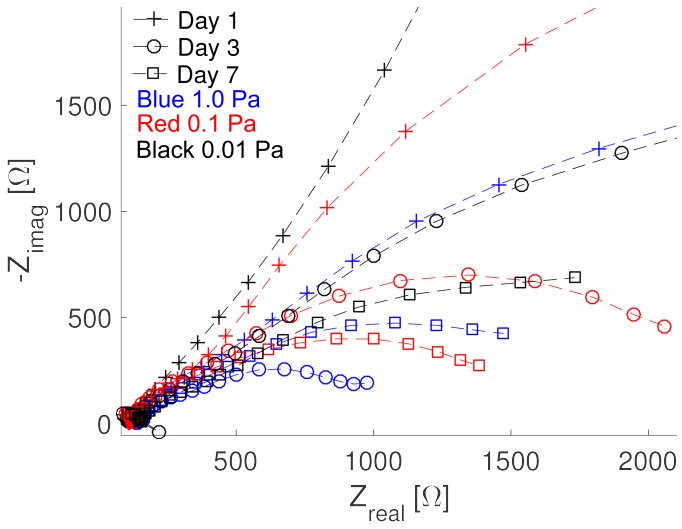

Figure 3-8: Temporal evolution of electrochemical impedance spectroscopy across shear. The decrease in electron transfer impedance follows the electron diffusion current closely as expected. There is an increase in impedance from day 3 to day 7 of the 1 Pa case but not the other two shear stress conditions. The absence of the increase in the 0.1 Pa and 0.01 Pa conditions clarifies that the steady state current seen in both electron diffusion and chronoamperometry has not started to decrease. The increase in impedance may be due to a decrease in redox proteins from loss of or death of cells, decrease in the biofilm pH which may cause a loss of conductivity and or metabolic activity [54, 6]. While the curves for day 1 do increase for all three conditions, they are not, and should not be, the same as those in Figure 3-7 because the measurement is taken 24 hours after inoculation.

activity.[53, 54, 6] While the curves for day 1 do increase for all three conditions, they are not, and should not be, the same as those in Figure 3-7 because the measurement is taken 24 hours after inoculation. Babauta and Beyenal [35] looked at impedance as a function of rotation rate. The rotation rate was changed on impulse and not with regards to continuous shear. A different approach was taken by Bonanni et al., to measure dependence of electron and substrate diffusion as well as substrate advection on limiting current.[16] Their work did not operate near maximum flux and subsequently was not intended to differentiate between the affects of momentum and mass transport.

The maximum current and thickness was higher than that found in studies on similar systems with different mass flux and shear rates. [55] Lower currents were found at lower shear rates. The thickness and surface roughness of the biofilms are

Table 3.3: Morphology and scaling parameters of biofilms

$\tau_{z\theta}$ [Pa]	H[μm]	Ra	k	τ_0	L
1	30.287	2.5067	6.81E+03	9.62E-04	402
0.1	41 ± 12	2.07	6.07E+03	1.14E-03	402
0.01	16 ± 3	1.36 ± 0.02	2.67E+03	2.65E-03	402

shown in Table 3.3 This is half the maximum thickness found in previous studies [56] though as mentioned earlier a higher current density than with other experiments with the same species. The independence of thickness and shear for the two higher shear rates agrees with previous studies showing independence at all shear on membrane aerated biofilms [57]. This disagrees with a similar study on biofilms developed *in vivo* from a river constriction pipe and analyzed using a rotating disk electrode.[58] Further work should be done to determine if this disagreement is from the non-constant mass flux or the multispecies nature of the biofilm. A further hypothesis is provided by noting that the independence is only seen with the 1.0 and 0.1 Pa conditions and, as will be shown through dimensional analysis, the 0.01 Pa case is not fully developed.

To provide further insight into the processes occurring within the biofilm we created a dimensionless model of the current and growth, shown in Figure 3-10. We fit the data to that of a logistic growth model as

$$\left(\frac{I}{nFAN}\right)^{1/2} = \frac{L}{1+\exp\left(-k(tYq_m - \tau_0)\right)} \tag{3.11}$$

The factor of $1/2$ in the dimensionless current accounts for the shear which constrains the volume described in Appendix B. The volume modifies the current following the Wiener model for porous media conductivity $\sigma_p \phi V$ where σ_p is the conducting pili conductance, ϕ is the biofilm porosity, and V is the volume [39]. The parameters are shown in Table . The resulting maximum value, L, of the curve exceeds unity indicating that there is something other than acetate that the bacteria are consuming to produce current which has been seen for other microbial fuel cells where the Coulombic efficiency meets or exceeds unity. The k value is proportional to a growth rate, as is clear from the decreasing value with increasing shear and current. The

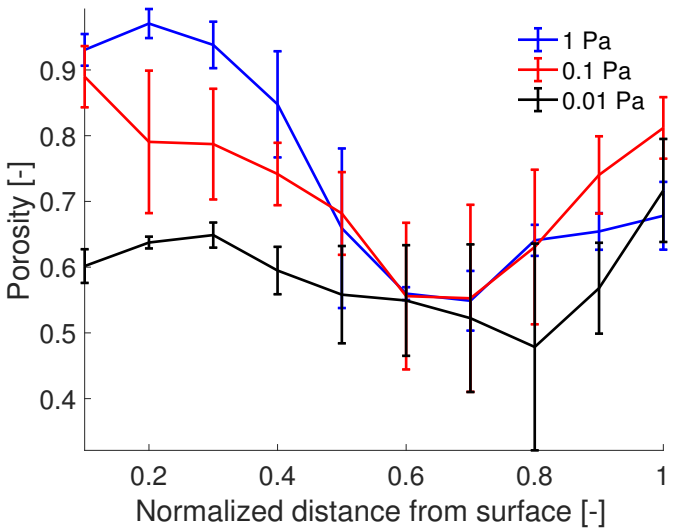

Figure 3-9: Mean porosity as a function of dimensionless distance taken from confocal microscopy images of the biofilms. The porosity decreases to a minimum at towards center of the biofilm at all three shear stress conditions while there is not a clear distinction between the 1 and 0.1 Pa conditions. The 0.01 Pa condition is different, providing evidence that it may not be fully developed. The lower porosity appears to be an artifact of the initial shear stress pattern as seen in Figure 3-3b. The porosity was calculated by merging the two images of AlexaFluor 594 and DAPI as described in the methods section, converting to binary in MATLAB and calculating the overall porosity on $212 \times 212\,\mu$m or $850 \times 850\,\mu$m images.

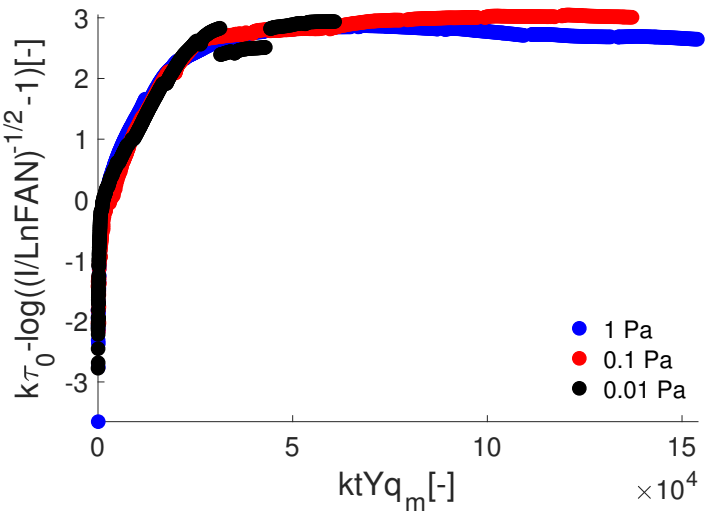

Figure 3-10: Dimensionless chronoamperometry at fixed mass flux and three shear stresses. The current is normalized to the theoretical current for fixed acetate flux ($5.35 \times 10^{-6}\,\mathrm{gCOD \cdot cm^{-2} \cdot s^{-1}}$) and a total transfer of electrons ($n = 8$) at three shear stresses tested of 1 Pa, 0.1 Pa and 0.01 Pa. The scaled growth time seems to account for most of the differences between each of the different shear stress.

midpoint, τ_0 is decreasing with increasing shear, again showing shear induced faster growth. The model does not predict the decay in current, the deviation of the 1.0 Pa condition from the 0.1 Pa shear stress condition. Yet, it does predict that this point is reached by $ktYq_m = 10^5$ or $t = 3.8$, 4.3 or 9.8 days for the 1.0, 0.1, and 0.01 Pa conditions respectively.

The optimal operation of a bioreactor includes the control of biofilm thickness and managing biofilm removal under shear.[27] In porous membrane bioreactors, the thickness of the biofilm is constrained by the size of the pores and both pumping and filtration efficiency decrease as a result.[59, 60, 61] To determine how shear impacts biofilm growth and detachment, we conducted the first long-term study on the effects of fluid flow history on biofilm growth and metabolism.[62] Furthermore, active transport of bacteria may increase current production similar to gravity sedimentation.[63] We show that the startup time and development time of the biofilm under shear are shortened at higher shear rates.

Biofilms under mechanical, thermal, and other forms of environmental stress change their metabolism.[23, 64, 65] Yet, separating these stressors has been diffi-

cult. A biofilm may respond to different stresses by increasing/decreasing cell mass production, cell production, and detachment.[33] Substrate utilization and current generation, both of which may be influence by shear stress, are the key figures of merit to be optimized for both wastewater treatment and microbial fuel cells. Current generation can be a proxy for metabolism though the relationship and efficiency is complex. [25] Under this hypothesis, we show that the biofilm increases its respiration rates under shear but at the cost of long-term stability.

As we noted in the description of the media, we did not balance the conductivity with increased acetate loading. Increased ion concentration should lead to higher current [66] but we find the opposite. This likely means that the difference in conductivity $\sim 1.2\,\mathrm{mS\,cm^{-1}}$ is not as significant as the impact of shear stress. Future testing should be done to see how changes in conductivity can diffuse through the biofilm.

3.4 Conclusion & Future Work

We performed a long-term study of the independent effect of shear stress on an electroactive biofilm. These biofilms are unique in that they do not rely on electron acceptor diffusion as they are "wired" to the electron acceptor thus leading to thicker biofilms. Similar to previous work [6], we propose that the maximum limitation of these biofilms is waste removal. We conclude that high shear rates lead to faster start-up times and higher metabolic rates at the cost of reduced waste removal. All fully-developed biofilms were roughly the same thickness and porosity. Further work should be done to probe the pH of these biofilms grown under different shearing conditions. Noting the importance of waste removal, future testing devices should include hydraulic conditions similar to the drained and undrained devices for testing poroelastic response of soils.

References

[1] Bruce E Logan. Exoelectrogenic bacteria that power microbial fuel cells. Nature Reviews Microbiology, 7(5):375–381, 2009.

[2] Derek R Lovley. Bug juice: harvesting electricity with microorganisms. Nature Reviews Microbiology, 4(7):497–508, 2006.

[3] Christin Koch and Falk Harnisch. Is there a specific ecological niche for electroactive microorganisms? ChemElectroChem, 3(9):1282–1295, 2016.

[4] DR Lovley and EJ Phillips. Rapid assay for microbially reducible ferric iron in aquatic sediments. Appl. Environ. Microbiol., 53(7):1536–40, 1987.

[5] CR Myers and KH Nealson. Bacterial manganese reduction and growth with manganese oxide as the sole electron acceptor. Science, 240(4857):1319–21, 1988.

[6] Sudeep C Popat and César I Torres. Critical transport rates that limit the performance of microbial electrochemistry technologies. Bioresource Technology, 215:265–273, 2016.

[7] Partha Jana, Krishna Katuri, Paul Kavanagh, Amit Kumar, and Dónal Leech. Charge transport in films of geobacter sulfurreducens on graphite electrodes as a function of film thickness. Physical Chemistry Chemical Physics, 16(19):9039–9046, 2014.

[8] Gemma Reguera, Kelly P Nevin, Julie S Nicoll, Sean F Covalla, Trevor L Woodard, and Derek R Lovley. Biofilm and nanowire production leads to increased current in geobacter sulfurreducens fuel cells. Appl. Environ. Microbiol., 72(11):7345–8, 2006.

[9] Elena Kipf, Julia Koch, Bettina Geiger, Johannes Erben, Katrin Richter, Johannes Gescher, Roland Zengerle, and Sven Kerzenmacher. Systematic screening of carbon-based anode materials for microbial fuel cells with shewanella oneidensis MR-1. Bioresource Technology, 146:386–392, 2013.

[10] Diana Pocaznoi, Amandine Calmet, Luc Etcheverry, Benjamin Erable, and Alain Bergel. Stainless steel is a promising electrode material for anodes of microbial fuel cells. Energy & Environmental Science, 5(11):9645, 2012.

[11] Xingwang Zhou, Xiaofen Chen, Hongying Li, Juan Xiong, Xiaoping Li, and Weishan Li. Surface oxygen-rich titanium as anode for high performance microbial fuel cell. Electrochimica Acta, 209:582–590, 2016.

[12] Z He, Shelley Minteer, and Largus T Angenent. Electricity generation from artificial wastewater using an upflow microbial fuel cell. Environmental Science and Technology, 39(14):5262–5267, 2005.

[13] Weihua He, Maxwell J Wallack, Kyoung-Yeol Kim, Xiaoyuan Zhang, Wulin Yang, Xiuping Zhu, Yujie Feng, and Bruce E Logan. The effect of flow modes and electrode combinations on the performance of a multiple module microbial fuel cell installed at wastewater treatment plant. Water Research, 105:351–360, 2016.

[14] Jian Li, Zheng Ge, and Zhen He. A fluidized bed membrane bioelectrochemical reactor for energy-efficient wastewater treatment. Bioresource Technology, 167:310–315, 2014.

[15] Qian Deng, Xinyang Li, Jiane Zuo, Alison Ling, and Bruce E Logan. Power generation using an activated carbon fiber felt cathode in an upflow microbial fuel cell. Journal of Power Sources, 195(4):1130–1135, 2010.

[16] Sebastian P Bonanni, Dan F Bradley, Germán D Schrott, and Juan Busalmen. Limitations for current production in geobacter sulfurreducens biofilms. ChemSusChem, 6(4):711–720, 2013.

[17] RS Renslow, Jerome T Babauta, PD Majors, and H Beyenal. Diffusion in biofilms respiring on electrodes. Energy Environ. Sci., 6(2):595–607, 2013.

[18] Van AS Wey, AL Cookson, TK Soboleva, NC Roy, McNabb, WC, A Bridier, R Briandet, and PR Shorten. Anisotropic nutrient transport in three-dimensional

single species bacterial biofilms. Biotechnology and Bioengineering, 109(5):1280–1292, 2011.

[19] Paul Stoodley, deBeer, Dirk, and Zbigniew Lewandowski. Liquid flow in biofilm systems. Appl Environ Microbiol, 60(8):2711–2716, 1994.

[20] G Liu, DA Tree, and MS High. Relationships between rotating disk corrosion measurements and corrosion in pipe flow. Corrosion, 50(8):584–593, 1994.

[21] Philippe Mandin, Th Pauporté, Ph Fanouillère, and D Lincot. Modelling and numerical simulation of hydrodynamical processes in a confined rotating electrode configuration. Journal of Electroanalytical Chemistry, 565(2):159–173, 2004.

[22] Benjamin G Levich. The theory of concentration polarisation. Discussions of the Faraday Society, 1:37–49, 1947.

[23] Y Liu and J-H Tay. Metabolic response of biofilm to shear stress in fixed-film culture. Journal of Applied Microbiology, 90(3):337–342, 2001.

[24] Colin Wardman, Kelly P Nevin, and Derek R Lovley. Real-time monitoring of subsurface microbial metabolism with graphite electrodes. Front Microbiol, 5:621, 2014.

[25] Hend MM Selim, Ahmed M Kamal, Dina MM Ali, and Rabeay YA Hassan. Bioelectrochemical systems for measuring microbial cellular functions. Electroanalysis, 2017.

[26] Paul Stoodley, Zbigniew Lewandowski, John D Boyle, and Lappin-Scott, Hilary M. Structural deformation of bacterial biofilms caused by short-term fluctuations in fluid shear: An in situ investigation of biofilm rheology. Biotechnology and Bioengineering, 65(1):83–92, 1999.

[27] Mark J Hammer, Jr and Mark J Hammer, Sr. Water and wastewater technology. Pearson Prentice Hall, 7 edition, 2012.

[28] Haydée Becerra, C Retamoso, and Digby D Macdonald. The corrosion of carbon steel in oil-in-water emulsions under controlled hydrodynamic conditions. Corrosion Science, 42(3):561–575, 2000.

[29] Richard Holdich. Fluid flow in porous media, chapter 3, pages 21–28. Midland Information Technology & Publishing, 2002.

[30] PC Carman. Fluid flow through granular beds. Chemical Engineering Research and Design, 75(0):S32–S48, 1997.

[31] Edward A Mason and AP Malinauskas. Gas Transport in Porous Media: The Dusty-Gas Model. Elsevier Science Publishing Company, INC, New York, NY, 1983.

[32] Esteve-Núñez, Abraham, Mary Rothermich, Manju Sharma, and Derek Lovley. Growth of geobacter sulfurreducens under nutrient-limiting conditions in continuous culture. Method Enzymol, 7(5):641–648, 2005.

[33] Carey D Nadell, Joao de Xavier, and Kevin R Foster. The sociobiology of biofilms. FEMS microbiology reviews, 33(1):206–224, 2009.

[34] MV Coppi, C Leang, SJ Sandler, and Derek R Lovley. Development of a genetic system for geobacter sulfurreducens. Applied and Environmental Microbiology, 67(7):3180–3187, 2001.

[35] Jerome T Babauta and Haluk Beyenal. Mass transfer studies of geobacter sulfurreducensbiofilms on rotating disk electrodes. Biotechnology and Bioengineering, 111(2):285–294, 2013.

[36] Laurence Soussan, Benjamin Erable, Marie-Line Delia, and Alain Bergel. The open circuit potential of geobacter sulfurreducens bioanodes depends on the electrochemical adaptation of the strain. Electrochemistry Communications, 33:35–38, 2013.

[37] P Bernabeu, Luc Tamisier, De A Cesare, and Adrien Caprani. Study of the adsorption of albumin on a platinum rotating disk electrode using impedance measurements. Electrochimica Acta, 33(8):1129–1136, 1988.

[38] Enrico Marsili, Janet B Rollefson, Daniel B Baron, Raymond M Hozalski, and Daniel R Bond. Microbial biofilm voltammetry: Direct electrochemical characterization of catalytic Electrode-Attached biofilms. Appl Environ Microb, 74(23), 2008.

[39] Strycharz-Glaven, Sarah, RM Snider, Guiseppi-Elie, A, and Leonard M Tender. On the electrical conductivity of microbial nanowires and biofilms. Energy Environ Sci, 4(11):4366–4379, 2011.

[40] Daniel R Bond, Strycharz-Glaven, Sarah, Leonard M Tender, and César I Torres. On electron transport through geobacter biofilms. ChemSusChem, 5(6):1099–1105, 2012.

[41] William G Characklis, Michael G Trulear, JD Bryers, and N Zelver. Dynamics of biofilm processes: Methods. Water Research, 16(7):1207–1216, 1982.

[42] Michael W Dunne. Bacterial adhesion: seen any good biofilms lately? Clin Microbiol Rev, 15(2):155–166, 2002.

[43] Kerstin Dolch, Joana Danzer, Tobias Kabbeck, Benedikt Bierer, Johannes Erben, Andreas H Förster, Jan Maisch, Peter Nick, Sven Kerzenmacher, and Johannes Gescher. Characterization of microbial current production as a function of microbe-electrode-interaction. Bioresource Technology, 157:284–292, 2014.

[44] Enrico Marsili, Jian Sun, and Daniel R Bond. Voltammetry and growth physiology of geobacter sulfurreducens biofilms as a function of growth stage and imposed electrode potential. Electroanalysis, 22(7-8):865–874, 2010.

[45] Michael Trulear and William G Characklis. Dynamics of biofilm processes. Journal (Water Pollution Control Federation), 54(9):1288–1301, 1982.

[46] James Wilking, Thomas Angelini, Agnese Seminara, Michael Brenner, and David Weitz. Biofilms as complex fluids. Mrs Bull, 36(5):385–391, 2011.

[47] Rachel Snider, Strycharz-Glaven, Sarah, Stanislav Tsoi, Jeffrey Erickson, and Leonard Tender. Long-range electron transport in geobacter sulfurreducens biofilms is redox gradient-driven. Proc National Acad Sci, 109(38):15467–15472, 2012.

[48] McLean, Jeffrey S, Greg Wanger, Yuri A Gorby, Martin Wainstein, McQuaid, Jeff, Shun' ichi Ishii, Orianna Bretschger, Haluk Beyenal, and Kenneth H Nealson. Quantification of electron transfer rates to a solid phase electron acceptor through the stages of biofilm formation from single cells to multicellular communities. Environmental Science and Technology, 44(7):2721–2727, 2010.

[49] DR Bond and Derek R Lovley. Electricity production by geobacter sulfurreducens attached to electrodes. Applied and Environmental Microbiology, 69(3):1548–1555, 2003.

[50] Falk Harnisch and Stefano Freguia. A basic tutorial on cyclic voltammetry for the investigation of electroactive microbial biofilms. Chemistry – An Asian Journal, 7(3):466–475, 2012.

[51] Hanno Richter, Kelly Nevin, Hongfei Jia, Daniel Lowy, Derek Lovley, and Leonard Tender. Cyclic voltammetry of biofilms of wild type and mutant geobacter sulfurreducens on fuel cell anodes indicates possible roles of OmcB, OmcZ, type IV pili, and protons in extracellular electron transfer. Energy Environ Sci, 2(5):506–516, 2009.

[52] Allen J Bard and Larry R Faulkner. Electrochemical Methods. John Wiley & Sons Incorporated, 2nd edition, 2001.

[53] Diwakar Kashyap, Prabhat K Dwivedi, Jitendra K Pandey, Young Kim, Gyu Kim, Ashutosh Sharma, and Sanket Goel. Application of electrochemical

impedance spectroscopy in bio-fuel cell characterization: A review. International Journal of Hydrogen Energy, 39(35):20159–20170, 2014. rotating disk.

[54] Ashley E Franks, Kelly P Nevin, Hongfei Jia, Mounir Izallalen, Trevor L Woodard, and Derek R Lovley. Novel strategy for three-dimensional real-time imaging of microbial fuel cell communities: monitoring the inhibitory effects of proton accumulation within the anode biofilm. Energy & Environmental Science, 2(1):113–119, 2009.

[55] Jerome T Babauta, Christopher A Beasley, and Haluk Beyenal. Investigation of electron transfer by geobacter sulfurreducensBiofilms by using an electrochemical quartz crystal microbalance. ChemElectroChem, 1(11):2007–2016, 2014.

[56] Ashley E Franks, Richard H Glaven, and Derek R Lovley. Real-Time spatial gene expression analysis within Current-Producing biofilms. ChemSusChem, 5(6):1092–1098, 2012.

[57] E Casey, B Glennon, and G Hamer. Biofilm development in a membrane-aerated biofilm reactor: Effect of flow velocity on performance. Biotechnology and Bioengineering, 67(4):476–486, 2000.

[58] Stéphanie Boulêtreau, Jean-Yves Charcosset, Jean Gamby, Emilie Lyautey, Sylvain Mastrorillo, Frédéric Azémar, Frédéric Moulin, and Frédéric Garabetian. Rotating disk electrodes to assess river biofilm thickness and elasticity. Water Research, 45(3):1347–1357, 2011.

[59] Stewart W Taylor and Peter R Jaffé. Biofilm growth and the related changes in the pysical properties of a porous medium 1. experimental investigation. Water Resources Research, 26(9):2153–2159, 1990.

[60] Stewart W Taylor and Peter R Jaffé. Substrate and biomass transport in a porous medium. Water Resources Research, 26(9):2181–2194, 1990.

[61] Alfred B Cunningham, William G Characklis, Feisal Abedeen, and David

Crawford. Influence of biofilm accumulation on porous media hydrodynamics. Environmental Science and Technology, 25(7):1305–1311, 1991.

[62] Ursula Telgmann, Harald Horn, and Eberhard Morgenroth. Influence of growth history on sloughing and erosion from biofilms. Water Research, 38(17):3671–3684, 2004.

[63] Tian Li, Lean Zhou, Yawei Qian, Lili Wan, Qing Du, Nan Li, and Xin Wang. Gravity settling of planktonic bacteria to anodes enhances current production of microbial fuel cells. Appl Energ, 198:261–266, 2017.

[64] Alice Rochex, Jean-Jacques Godon, Nicolas Bernet, and Renaud Escudié. Role of shear stress on composition, diversity and dynamics of biofilm bacterial communities. Water Research, 42(20):4915–4922, 2008.

[65] William J Costerton, Zbigniew Lewandowski, Douglas E Caldwell, Darren R Korber, and Lappin-Scott, Hilary M. Microbial biofilms. Annual Reviews in Microbiology, 49(1):711–745, 1995.

[66] Timothy D Harrington, Jerome T Babauta, Emily K Davenport, Ryan S Renslow, and Haluk Beyenal. Excess surface area in bioelectrochemical systems causes ion transport limitations. Biotechnology and Bioengineering, 112(5):858–866, 2015.

Chapter 4

Conclusion

We show that a single platform can be used to analyze biofilms from initiation to decay and death. Growing a biofilm has been possible in other platforms for the last 400 years,[1] they are hard to prevent. Yet, the analytical tools necessary to differentiate them from their planktonic states have only been advanced over the last 40 years.[1] Confocal microscopy provides an unprecedented window into the structure of biofilms. Combining microscopy and computer vision with microfluidics in the early 2000s increased the understanding of biofilm initiation.[2] While rotating disk electrodes had been used to probe biofilm transport properties they had not been used to assess the health and metabolic activity of a biofilm.[3] While not representative of all bacterial species, electroactive bacteria include many δ-proteobacteria including *Pseudomonas aeruginos* which as been a model biofilm former since the term was first coined.[1] Furthermore, many studies, including those using rotating disks, on biofilms had not managed to separate substrate stress from shear stress. Our results show that this tool should be used to create the next set of breakthroughs in understanding biofilm dynamics.

Mass transport limiting current, both over a range of rotation rates and over time, as well as cyclic voltammetry can be used to determine the onset and quantify the area of bacterial adhesion to metals. The use of a rotating disk electrode refines the use of chronoamperometry used by Boulang-Petermann et al., [4] using controlled flux to the surface. We note that deviation from the Levich curve does not arise

from the same physical mechanisms exhibited by mammalian cells or high-density nano-particles. Stiffness is likely not a contributing factor to the deviation as both a stiff gram-positive and a less-stiff gram-negative bacterial strain exhibit similar behavior. Further examination of the effect of particle stiffness could be done using polymers like PDMS. Further, viscosity does not appear to change due to the presence of bacteria. Another difference between inert particles and bacteria is the soft layers on their surface which may be investigated using mutant strains, fixation or various salinity.[5]

We conclude that the deviation from the Levich curve is due to adhesion of bacteria and proteins to the surface of the electrode. The rotating disk electrode (RDE) is a useful tool to study bacterial adhesion under flow and at a fixed potential. While other tools used to measure adhesion are very accurate and sensitive, they are trade-offs not faced with an RDE.[6, 7] For example, microfluidic systems are limited to small working areas and small sample volumes which may limit the accessible range of transport regimes and increase cell-cell interaction unintentionally, thereby changing adhesive properties.[7] A rotating disk electrode can be scaled without changing the procedures or physical mechanisms of action or accuracy.[8] Additionally, while quartz-crystal micrography is very accurate in measuring adhered mass but cannot measure area it is also possible to incorporate a quartz-crystal microbalance into an RDE.[9]

Results of this study can be utilized to investigate the influence of flow conditions on bacterial adhesion to various electrochemically active surfaces. These techniques may be useful for addressing Nealson's hypothesis [10, 11] that surface polarization affects bacterial adhesion since limiting current occurs over a range of potentials. These methods may also be useful in determining if surface polarization is useful for preventing biofouling or using surface polarization and stirring to decrease start-up time in bioreactors.[12]

We performed a long-term study of the independent effect of shear stress on an electroactive biofilm. These biofilms are unique in that they do not rely on electron acceptor diffusion as they are "wired" to the electron acceptor thus leading to thicker

biofilms. Similar to previous work [13], we propose that the maximum limitation of these biofilms is waste removal. The additional understanding from this work is that high shear rates lead to faster start-up times and higher metabolic rates at the cost of reduced waste removal. All the biofilms were roughly the same thickness and porosity. Further work should be done to probe the pH of these biofilms grown under different shearing conditions. Noting the importance of waste removal, future testing devices should include hydraulic conditions similar to the drained and undrained devices for testing poroelastic response of soils.

References

[1] Niels Høiby. A personal history of research on microbial biofilms and biofilm infections. Pathogens Dis, 70(3):205–211, 2014.

[2] Henk J Busscher and Henny C van der Mei. Microbial adhesion in flow displacement systems. Clin Microbiol Rev, 19(1):127–141, 2006.

[3] Hend MM Selim, Ahmed M Kamal, Dina MM Ali, and Rabeay YA Hassan. Bioelectrochemical systems for measuring microbial cellular functions. Electroanal, 2017.

[4] Boulangé-Petermann, Laurence, Bellon-Fontaine, Marie-Nöelle, and Bernard Baroux. An electrochemical method for assessing biodeposition on stainless steel. Journal of Microbiological Methods, 21(1):83–96, 1995.

[5] Naga Dingari and Cullen R Buie. Theoretical investigation of bacteria polarizability under direct current electric fields. Langmuir, 30(15):4375–4384, 2014.

[6] Margot Vigeant, Roseanne M Ford, Michael Wagner, and Lukas K Tamm. Reversible and irreversible adhesion of motile escherichia coli cells analyzed by total internal reflection aqueous fluorescence microscopy. Appl Environ Microb, 68(6):2794–2801, 2002.

[7] Hannah H Tuson and Douglas B Weibel. Bacteria–surface interactions. Soft Matter, 9(17):4368, 2013.

[8] Philippe Mandin, Th Pauporté, Ph Fanouillère, and D Lincot. Modelling and numerical simulation of hydrodynamical processes in a confined rotating electrode configuration. Journal of Electroanalytical Chemistry, 565(2):159–173, 2004.

[9] Ying Liu, Antonio Berná, Victor Climent, and Juan Feliu. Real-time monitoring of electrochemically active biofilm developing behavior on bioanode by using EQCM and ATR/FTIR. Sensors and Actuators B: Chemical, 209:781–789, 2015.

[10] KH Nealson and SE Finkel. Electron flow and biofilms. Mrs Bulletin, 2011.

[11] Kenneth H Nealson and Annette R Rowe. Electromicrobiology: realities, grand challenges, goals and predictions. Microbial Biotechnology, 9(5):595–600, 2016.

[12] Xin Wang, Yujie Feng, Nanqi Ren, Heming Wang, He Lee, Nan Li, and Qingliang Zhao. Accelerated start-up of two-chambered microbial fuel cells: effect of anodic positive poised potential. Electrochimica Acta, 54(3):1109–1114, 2009.

[13] Sudeep C Popat and César I Torres. Critical transport rates that limit the performance of microbial electrochemistry technologies. Bioresource Technology, 215:265–273, 2016.

Appendix A

Rotating Disk Electrode Theory

A.0.1 Hydrodynamics

We briefly summarize the results of Levich[1] and von Kármán[2] that describe the fluid transport, mass transport, and current measurement that is the basis for this work (see Equation A.21). von Kármán solved for the fluid flow in a near disk region of the rotating disk system. He modeled a disk of radius a rotating at speed frequency ω in an infinite fluid bath. Starting with an incompressible Newtonian form of the Navier-Stokes equation

$$(\mathbf{u} \cdot \nabla)\mathbf{u} = -\frac{1}{\rho}\nabla p + \nu\nabla^2\mathbf{u}, \tag{A.1}$$

where p is the pressure, ρ is the density, ν is the viscosity and in cylindrical coordinates $\langle \hat{r}, \hat{\phi}, \hat{z} \rangle$ the velocity is

$$\mathbf{u} = rf(z)\hat{r} + rg(z)\hat{\phi} + h(z)\hat{z} \tag{A.2}$$

The $\hat{r}$ and $\hat{z}$ components tend to 0 and the ϕ component to ωr at the surface of the disc due to the no-slip condition. As $z \to \infty$ away from the plate, $f, g \to 0$ yet $h \to c$, a constant, to satisfy continuity. Scaling the velocity such that

$$\mathbf{u} = r\omega F(\zeta)\hat{r} + r\omega G(\zeta)\hat{\phi} + (\nu\omega)^{1/2}H(\zeta)\hat{z} \tag{A.3}$$

where ζ is the dimensionless depth

$$\zeta = \left(\frac{\omega}{\nu}\right)^{1/2} z. \tag{A.4}$$

After substitution and scaling, the system to be solved is

$$\begin{aligned} F^2 - G^2 + HF' &= F'', \\ 2FG + HG' &= G'', \\ HH' + 2F' &= P', \\ 2F + H' &= 0 \end{aligned} \tag{A.5}$$

von Kármán's solution was a Taylor series for near disc $z \leq \nu^{1/2}\omega^{-1/2}$. Cochran corrected von Kármán's solution since it erred in satisfying the no-slip condition [2]. He also developed a solution that held in the bulk solution using an asymptotic expansion of F, G, and H,

$$\Psi(\zeta) = \sum a_n e^{-cn\zeta}, \tag{A.6}$$

where Ψ is substituted for F, G, H. Benton showed that the matching between the near disc and bulk solution was not necessary and one could use the exponential expansion in the near wall case [3].

The flow as described only has a z component away from the surface of the disk gradually gaining a rotational and radial component the closer one gets to the surface, shown in Figure A-1

The fluid shear force at the surface is

$$\tau_{z\theta} = \mu\left(\frac{\partial u_\theta}{\partial z} + \frac{1}{r}\frac{\partial u_z}{\partial \theta}\right) = \rho^{1/2}\mu^{1/2}\omega^{3/2} r G'\left(\left(\frac{\omega}{\nu}\right)^{1/2} z\right) \simeq 0.6159\rho^{1/2}\mu^{1/2}\omega^{3/2} r \tag{A.7}$$

The value of $G'(0) = -0.6159$ is from the expansion Eq. A.6 as corrected by Benton [3]. The shear can be made dimensionless by dividing by the fluid inertia,

$$\frac{\tau_{z\theta}}{\frac{1}{2}\rho U^2} = G'(0) 2\sqrt{2} Re_D^{-1/2}, \tag{A.8}$$

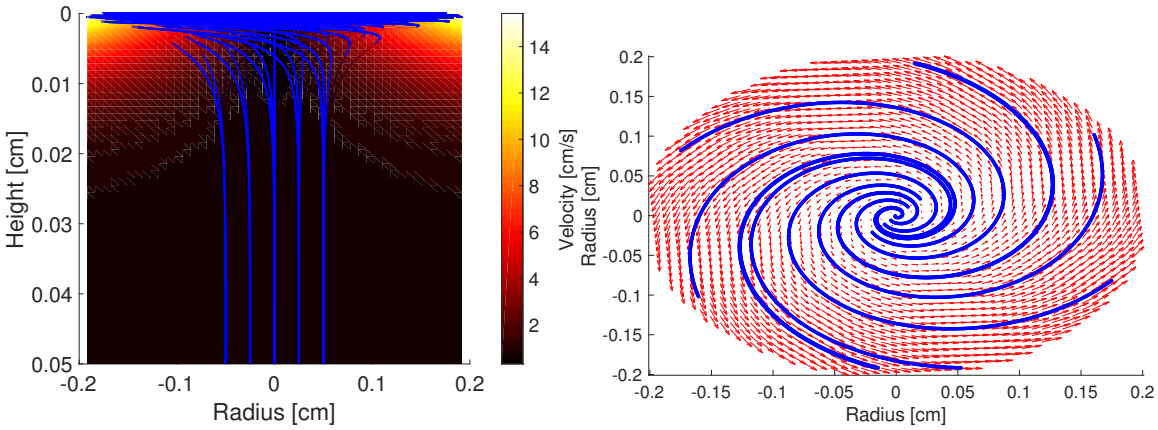

(a) Streamlines overlayed on a velocity mag-(b) Vector Streamlines at 739 RPM or nitude plot for a rotation rate of 739 RPM1046 s^{-1}
within 0.1 cm from the surface of the disk.

Figure A-1: Velocity as described by Kármán

where the Reynolds number is defined as

$$Re_D = \frac{UL_c}{\nu} = \frac{(\omega r)(2r)}{\nu} \tag{A.9}$$

The models for the rotating disk system work when the boundary layers formed on ceiling, floor, and walls of the chamber do not meet those of the disk. [4, 5] That is the floor and ceiling must be far enough away and the disc radius to chamber radius ratio must be much less than 0.9; here it is 0.06. Turbulence is not a concern in RDE systems since it occurs around $Re_D \sim 2 \times 10^5$ or 7600 rpm for a 5 mm dia. disk[6]. Turbulent systems are also typically not used in engineered biofilm systems since biofilms cannot withstand such shear. Steady-state is reached within 2% by $2\omega t$ or 22-0.008 s [3].

A.0.2 Mass Transport

Levich used the asymptotic expansion for the velocity in his solution to the advection-diffusion equation in 2D to develop an expression for the diffusion layer

above rotating disk electrodes [1]. The advection-diffusion equation is

$$\frac{\partial c}{\partial t} + v_r \frac{\partial c}{\partial r} + \frac{v_\phi}{r} \frac{\partial c}{\partial \phi} + v_z \frac{\partial c}{\partial z} = D_0 \left(\frac{1}{r} \frac{\partial}{\partial r} \left(r \frac{\partial c}{\partial r} \right) + \frac{1}{r^2} \frac{\partial^2 c}{\partial \phi^2} + \frac{\partial^2 c}{\partial z^2} \right), \tag{A.10}$$

where D_0 is the diffusivity of the solute in question. If the system has reached steady-state, then the first term on the left hand side is 0. Since $c(\phi) = c(\phi + 2\pi)$ any derivatives in ϕ are 0. It follows that the advection-diffusion equation reduces to:

$$v_r \frac{\partial c}{\partial r} + v_z \frac{\partial c}{\partial z} = D_0 \left(\frac{1}{r} \frac{\partial}{\partial r} \left(r \frac{\partial c}{\partial r} \right) + \frac{\partial^2 c}{\partial z^2} \right) \tag{A.11}$$

Very close to the surface, the radial change in concentration goes to zero,

$$\lim_{z \to 0} \frac{\partial c}{\partial r} = 0 \tag{A.12}$$

The flux at the surface is then found by solving for $\frac{\mathrm{d}c}{\mathrm{d}z}$ and results in

$$N = D_0 \left. \frac{\mathrm{d}c}{\mathrm{d}z} \right|_{z=0} \simeq 0.62 c_\infty \nu^{-1/6} D_0^{2/3} \omega^{1/2} \tag{A.13}$$

Combining this with the concept of Nernst diffusion limited current density,

$$j = F z_i D_0 \frac{c_\infty - c_0}{\delta'} \tag{A.14}$$

the asymptotic diffusion length is:

$$\delta' = \frac{N}{c_\infty D_0} = 1.61 \left(\frac{D_0}{\nu} \right)^{1/3} \left(\frac{\nu}{\omega} \right)^{1/2} \tag{A.15}$$

This resulted in mass transport to a rotating disk showing a fast drop in concentration over one diffusion length so it is a 'diffusion layer,' though not of fixed concentration nor static concentration. Mandin et al., showed by experimental and a numerical simulation of the Navier-Stokes equation around a micro-electrode that Cochran's 3rd order Taylor series expansion underestimated the velocity gradient by 40% within the mass transport boundary layer at 100 rad$\cdot$ s^{-1} [4]. By using this erroneous velocity

expansion, they showed that Levich's model overestimates the mass transport by 3% [4]. Levich's solution is useful for experimental computation so we use Cochran's exponential solution to 50th order as recommended by Benton. Substituting Cochran's exponential solution in the expression for mass flux results in

$$N = c_\infty \nu^{-1/6} D_0^{2/3} \omega^{1/2} \left(cSc^{-1/3} J^{-1} \right) \tag{A.16}$$

where the first four terms are identical to Levich's solution and

$$\int_0^\infty \exp Sc \left(-x + \sum_{j=1}^{N} \frac{b_j}{j} \left(1 - e^{-jx} \right) \right) dx. \tag{A.17}$$

At $N = 1$, the result can be approximated as an improper Gamma function for large Sc. At $N = 2$ and $Sc = 1$ the integral can be approximated as an error function. Yet, there is no closed form for $N > 2$. Using adaptive quadrature we have calculated this for biologically related chemicals, the acetate ion, acetic acid, α-D-glucose, sucrose, and the proton at 25 °C out to $N = 60$. Convergence is reached for all four chemicals is reached at $N = 23$ (cf. Figure [A-2]). The disadvantage of this method compared to the Levich model is that the integral depends on the solute diffusivity and must be computed, yet modern computers can do this in 0.1 seconds (MATLAB, 2.4GHz Processor, 4Gb ram).

The average relative error between our calculated term and Levich's approximation is 3.6% in agreement with Mandin et al.[4] The greatest difference is for the proton of 6.89% which is significant noting that proton conduction is viewed as a limiting factor in power production for MFCs.

The maximum current, Equation A.18, that can be obtained at a given rotation rate is a product of the number of electrons transferred per reaction, n, Faraday's constant, F, the projected area, A, and the flux to the surface, N,

$$i_{lim} = n_e F A N. \tag{A.18}$$

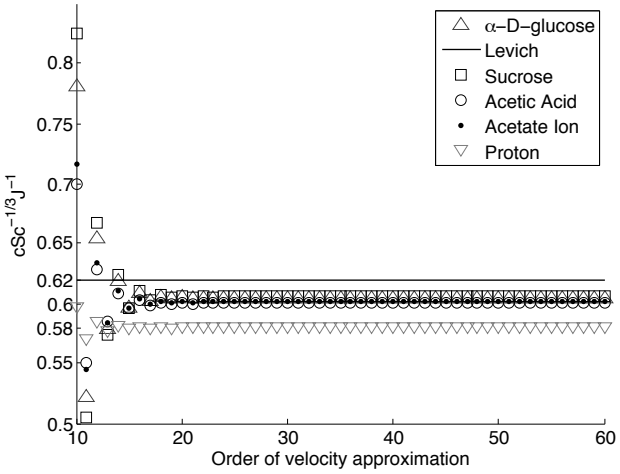

Figure A-2: The correction and convergence to Levich's mass transfer model of six biologically relevant chemicals based on diffusivities in literature. Convergence is reached between a 20 and 30 order approximation. While the error is only between 2 – 6% as shown in Table A.1, the rapid convergence shows this source of error is unnecessary.

Table A.1: Coefficients of the Levich expression for mass flux for four biologically relevant diffusivities. The percent relative error of the Levich expression is $\delta = |cSc^{-1/3}J^{-1} - 0.62|/cSc^{-1/3}J^{-1} \times 100$. Values from [7]

	Acetate	Acetic Acid	α-D-glucose	Sucrose	Proton
Diffusivity $[10^{-5}\,\mathrm{cm^2 s^{-1}}]$	1.089	1.29	0.67	0.52	9.311
$cSc^{-1/3}J^{-1}$	0.6012	0.6001	0.6042	0.6056	0.5800
$\delta\%$	3.12	3.32	2.60	2.37	6.89

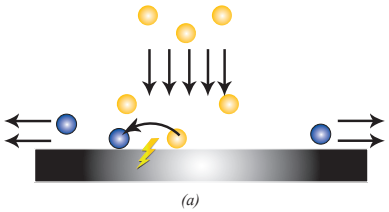

Figure A-3: A graphical representation of mass transport limited reactions on the surface of a rotating disk. The reduced form of a molecule, shown in yellow, is transported with the fluid to the surface of the disk, is oxidized to the blue form with the transfer of electrons to the disk and is transported radially away from the disk.

Or by substituting Equation A.16 into Equation A.18[8]

$$i_{lim} = n_e F A c_0 \nu^{-1/6} D_0^{2/3} \omega^{1/2} \left(c \mathrm{Sc}^{-1/3} J^{-1} \right). \tag{A.19}$$

Mass-transport limiting current is the current when the electrochemical reaction is limited solely by reactant transport to the electrode and can be used to measure diffusivity of the reacting species. This is shown graphically in Figure A-3 The Levich curve is the result of plotting $\log(i_{lim})$ vs $\log(\omega)$ and should result in a straight line with slope 1/2.[8]

If the mass transfer coefficient, k_m, is defined from the limiting current as

$$i_{lim} = nFAk_m c_0 \tag{A.20}$$

then the Levich equation, Equation A.19, can be rewritten in dimensionless form as

$$\frac{k_m R}{D_0} = \left(\frac{D_0}{\nu} \right)^{1/3} \left(\frac{\rho \omega R^2}{\mu} \right) = \mathrm{Sc}^{1/3} \mathrm{Re}^{1/2}, \tag{A.21}$$

where the Sherwood number is $\mathrm{Sh} = k_m R / D_0$, and the Reynolds number is $\mathrm{Re} = \omega R^2 / \nu$.

References

[1] Benjamin G Levich. The theory of concentration polarisation. Discussions of the Faraday Society, 1:37–49, 1947.

[2] WG Cochran. The flow due to a rotating disc. Mathematical Proceedings of the Cambridge Philosophical Society, 30(3):365–375, 1934.

[3] Edward R Benton. On the flow due to a rotating disk. Journal of Fluid Mechanics, 24:781–800, 1966.

[4] Philippe Mandin, Th Pauporté, Ph Fanouillère, and D Lincot. Modelling and numerical simulation of hydrodynamical processes in a confined rotating electrode configuration. Journal of Electroanalytical Chemistry, 565(2):159–173, 2004.

[5] JW Daily and RE Nece. Chamber dimension effects on induced flow and frictional resistance of enclosed rotating disks. Journal of Basic Engineering, 82(1):217, 1960.

[6] N Gregory, JT Stuart, and WS Walker. On the stability of Three-Dimensional boundary layers with application to the flow due to a rotating disk, 1955. dynamic instability -Concave unstable/convex stableinflectional stability-A point of inflection is necessary and sufficient for 2D instablitiy in boundaries and channels; or infinite Re, Viscous Instability.

[7] William M Haynes. CRC handbook of chemistry and physics. CRC Press, 2014.

[8] Allen J Bard and Larry R Faulkner. Electrochemical Methods. John Wiley & Sons Incorporated, 2nd edition, 2001.

Appendix B

Shear Constraints on poroelastic media

Modeling biofilms can be approached using either continuum or discreet methods.[1] [2] Within continuum approaches, biofilms have been modeled as multiphase flows [3] or poroelastic solids with fluid intrusion [4]. We follow the poroelastic solid with fluid intrusion approach as we are looking at bulk properties of height and global porosity versus surface roughness, dispersion, tortuosity. No satisfactory physics of fracture exist to the best of the authors' knowledge and the best models for fracture follow discreet methods. [5]The upper bound on the volume is set by shear stress on a poroelastic media is found using the model by Gopinath and Mahdevan [6] that the response time for a poroelastic structure under shear loading should go as

$$t_p \sim \frac{\mu h^2}{k_p \phi E}. \tag{B.1}$$

This can be rewritten in terms of a velocity assuming that the response is on the same order as the fluid transit time across the disk,

$$1 \sim \frac{\tau h^2}{k_p \phi E}, \tag{B.2}$$

or solving for the height, h,

$$h = \frac{k_p \phi E}{\rho^{1/2} \mu^{1/2} \omega^{3/2} r c^3 \sum_1^n n a_n e^{-c\zeta n}}. \tag{B.3}$$

where the summation and constant c both come from von Kármán's expression for velocity[7] When integrated around the radius of the disk, this results in a maximum volume of

$$V_{max} = \frac{4}{3}\pi \left(\frac{k_p \phi_0 E r^3}{\rho_f \omega^2 c^3 \sum_1^n n a_n} \right)^{1/2} \tag{B.4}$$

where we assumed a first order Taylor expansion of the exponential as it drops of rapidly from the surface of the disk.

References

[1] Herman Eberl, Eberhard Morgenroth, Daniel Noguera, Cristian Picioreanu, Bruce E Rittmann, Mark C M van Loosdrecht, and Oskar Wanner. Mathematical Modeling of Biofilms. Technical Report 18, London, UK, 2006.

[2] James Wilking, Thomas Angelini, Agnese Seminara, Michael Brenner, and David Weitz. Biofilms as complex fluids. Mrs Bull, 36(5):385–391, 2011.

[3] Chen Chen, Shuyu Hou, Dacheng Ren, Mingming Ren, and Qi Wang. 3-D spatio-temporal structures of biofilms in a water channel. Mathematical Methods in the Applied Sciences, 38(18):n/a–n/a, 2014.

[4] CS Laspidou, LA Spyrou, N Aravas, and BE Rittmann. Material modeling of biofilm mechanical properties. Mathematical Biosciences, 251:11–15, 2014.

[5] Jason D Chambless and Philip S Stewart. A three-dimensional computer model analysis of three hypothetical biofilm detachment mechanisms. Biotechnology and Bioengineering, 97(6):1573–1584, August 2007.

[6] A. Gopinath and L. Mahadevan. Elastohydrodynamics of wet bristles, carpets and brushes. Proc Royal Soc Lond Math Phys Eng Sci, 467(2130):1665–1685, 2011.

[7] W G Cochran. The flow due to a rotating disc. Mathematical Proceedings of the Cambridge Philosophical Society, 30(03):365, July 1934.